nature microbiology

Article

https://doi.org/10.1038/s41564-026-02526-w

Lack of ancestral SARS-CoV-2 imprinting promotes Omicron sublineage BA.3.2.2 infection in children

Received: 28 June 2026

Accepted: 28 September 2026

Published online: 26 October 2026

Check for updates

Xiao Niu[1,2,3,14], Dan Xiong[4,14], Peizhuo He[2], Lingling Yu[2], Yutong Li[1,2], Xingan Cai[1,2], Ran An[2], Yao Wang[2], Ruoxi Kong[1,2], Yuanling Yu[2], Jing Wang[2], Qianran Wang[2], Juan Huang[5], Binmao Zhang[6], Tianen Zhu[6,7], Tianyuan Zhao[6,8], Jianheng Huang[6,8], Fanchong Jian[1], Fei Shao[2], Zhimin Huang[9], Xiaosu Chen[10], Zhongyang Shen[11], Ronghua Jin[12], Zhengde Xie[5], Xiangpeng Chen[5] ✉, Xiaotian Tan[6] ✉ & Yunlong Cao[1,2,13] ✉

The ongoing SARS-CoV-2 evolution is constrained by population-level immune imprinting. Recent genomic surveillance revealed an unexpected demographic shift with the Omicron sublineage BA.3.2.2 being predominant in paediatric populations globally. Here we show that this paediatric susceptibility arises from the absence of immune imprinting against ancestral SARS-CoV-2 Wuhan strain. Serological analyses reveal a failure to neutralize BA.3.2.2 in young children with no ancestral strain exposure. Single-B-cell sequencing analyses demonstrate that BA.3.2.2 evades Omicron-specific Class 1/4 neutralizing antibodies that target the ACE2-binding site, encoded by immunoglobulin heavy-chain variable (IGHV) germline genes *IGHV2-5* and *IGHV5-51*, which dominate in weakly imprinted individuals. BA.3.2.2 remains susceptible to broadly cross-reactive Class 1 antibodies, encoded by *IGHV3-53/66*, typically enriched in adults with strong Wuhan-strain imprinting, such as mRNA vaccine recipients. Together, these findings show that classic immune imprinting provides superior protection against a highly divergent variant, explaining the age-biased transmission of BA.3.2.2, and informing future paediatric vaccination strategies.

The evolutionary landscape of severe acute respiratory syndrome coronavirus 2 (SARS-CoV-2) has been characterized by continued adaptation of Omicron-derived lineages under widespread population immunity. During this period, the JN.1 descendant NB.1.8.1 and the recombinant lineage XFG became the major circulating variants since 2025[1–6]. The evolutionary success of both XFG and NB.1.8.1 is consistent with a broader pattern of incremental Omicron evolution, in which new variants acquire drifting mutations that reduce antibody neutralization while maintaining optimal human angiotensin-converting enzyme 2 (hACE2) receptor binding[2–4,7].

By contrast, the BA.3.2 lineage and its descendants emerged as highly divergent saltation variants[6,8,9]. First detected in Southern Africa in 2024 and later reported across multiple continents, BA.3.2 carries more than 50 spike mutations relative to BA.3 and more than 40 relative to JN.1, consistent with a saltation-like evolutionary pattern, potentially after prolonged intrahost evolution[10]. Consistent with this, naive animal immunization further revealed that BA.3.2.2 is antigenically distinct from JN.1-lineage viruses[3,11,12]. Despite this antigenic divergence, BA.3.2.2 has remained less prevalent than XFG or NB.1.8.1, possibly reflecting fitness costs such as altered spike conformation, reduced entry efficiency or slower replication[3]. These features make BA.3.2.2 an unusual lineage with substantial antigenic distinction but limited overall spread.

A full list of affiliations appears at the end of the paper. ✉e-mail: chenxp1111@163.com; xt.tan@siat.ac.cn; yunlongcao@pku.edu.cn

https://doi.org/10.1038/s41564-026-02526-w

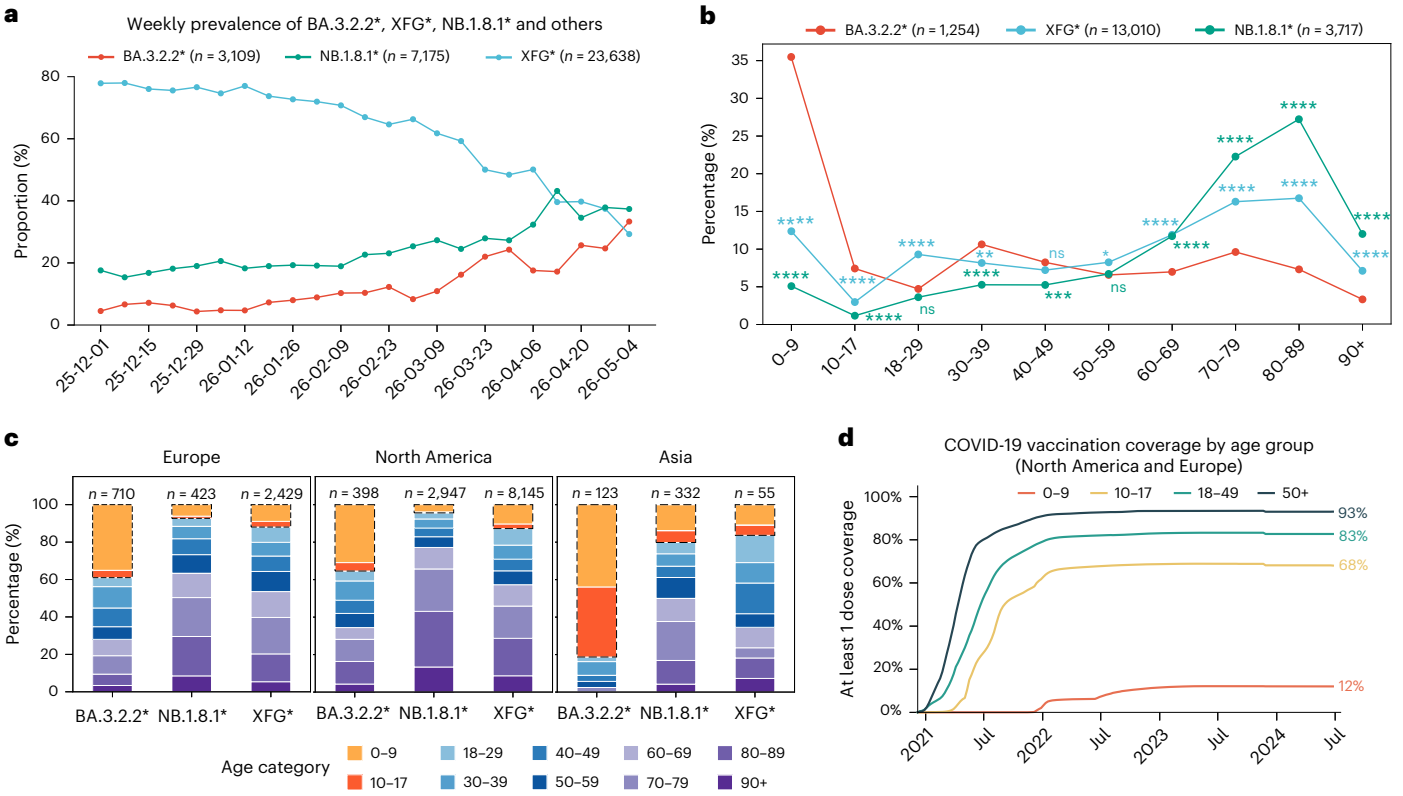


Fig. 1 | BA.3.2.2 is enriched in paediatric populations with low ancestral-strain exposure. a, Global weekly proportions of NB.1.8.1, XFG and BA.3.2.2 sublineages. **b**, Global age distribution of NB.1.8.1, XFG and BA.3.2.2 sublineages. **c**, Bar plots showing the age distribution of BA.3.2.2, NB.1.8.1 and XFG sublineages globally and across continents. The group aged 17 years or younger is circled with dashed black outlines. Data in **a**–**c** were obtained from GISAID and include records collected between 1 December 2025 and 24 May 2026. An asterisk following a lineage name (BA.3.2.2*, NB.1.8.1* and XFG*) denotes the parental lineage together with all of its designated descendant lineages. In **a**–**c**, *n* represents the number of records included in the corresponding GISAID analysis. **d**, Age-stratified vaccine coverage in major countries. Vaccination data were obtained from ECDC, the US CDC and Canada.ca. Broadly defined age groups, including groups such as under 60 years and 18–69 years, were excluded. Two-sided chi-square tests were used in **b**. $^{*}P < 0.05$, $^{**}P < 0.01$, $^{***}P < 0.001$, $^{****}P < 0.0001$; n.s., not significant ($P > 0.05$).

However, BA.3.2.2 has shown a marked increase in prevalence across multiple regions since late 2025, with continued global expansion during early 2026[8,13–16]. More importantly, genomic surveillance identified a profound epidemiological anomaly: BA.3.2.2 infections exhibit a dramatic enrichment in paediatric populations[17,18]. Generally, infectious respiratory diseases caused by SARS-CoV-2 variants heavily burden older populations owing to immunosenescence, cumulative comorbidities and waning immunity[19,20]. The inversion of this demographic vulnerability pattern suggests a highly specific immunological interaction between the unprecedented mutational profile of BA.3.2.2 and the distinct immunological histories of children.

Immunological naivety provides an intuitive explanation for the apparent enrichment of BA.3.2.2 in younger populations. Children have generally had fewer SARS-CoV-2 exposures than adults, and might therefore be more susceptible to a lineage that is antigenically distant from previously circulating variants. However, a comparable age skew was not observed during the major antigenic transition from XBB-lineage viruses to BA.2.86/JN.1, despite the broad humoral immune escape and antigenic distinctiveness of the latter lineage. This contrast argues against immunological naivety alone as the primary driver of BA.3.2.2 enrichment in children.

From another perspective, fewer and later exposures to ancestral-strain vaccines in children also imply weaker immune imprinting. In principle, weaker ancestral-strain imprinting would be expected to favour broader and more flexible neutralizing responses to antigenically drifted Omicron lineages[21–28]. The preferential enrichment of BA.3.2.2 in younger individuals, therefore, raises the possibility that this lineage exploits a more specific gap in the antibody landscape of individuals with limited ancestral-strain imprinting, whereas strongly imprinted adults may retain antibody specificities that better neutralize BA.3.2.2. This paradox prompted an investigation into whether imprinting-dependent differences in antibody repertoires underlie the age-associated spread of BA.3.2.2.

Results

BA.3.2.2 age bias

To characterize the age-associated epidemiology of BA.3.2.2, we analysed global SARS-CoV-2 sequence metadata from the GISAID EpiCoV database. BA.3.2.2 showed a marked increase in prevalence during early 2026 (Fig. 1a). Age-stratified analysis showed that XFG and NB.1.8.1 displayed conventional demographic profiles, with the proportion of reported sequences increasing across adult age groups and peaking in older adults. By striking contrast, BA.3.2.2 was significantly enriched in individuals aged 17 years or younger, with the strongest enrichment observed in children aged 0–9 years (Fig. 1b). This paediatric enrichment was consistently observed across Europe, North America and Asia, and was also reproduced at the individual-country level (Fig. 1c and Extended Data Fig. 1a).

To examine whether this age bias coincided with differences in ancestral-strain exposure, we further compiled retrospective age-stratified coronavirus disease 2019 (COVID-19) vaccination coverage from the European Centre for Disease Prevention and Control, the US Centers for Disease Control and Prevention and the Government of Canada. Across countries, children consistently showed substantially lower and later uptake of ancestral-strain vaccines than adults, with the lowest coverage observed in the youngest age groups (Fig. 1d and Extended Data Fig. 2a).

https://doi.org/10.1038/s41564-026-02526-w

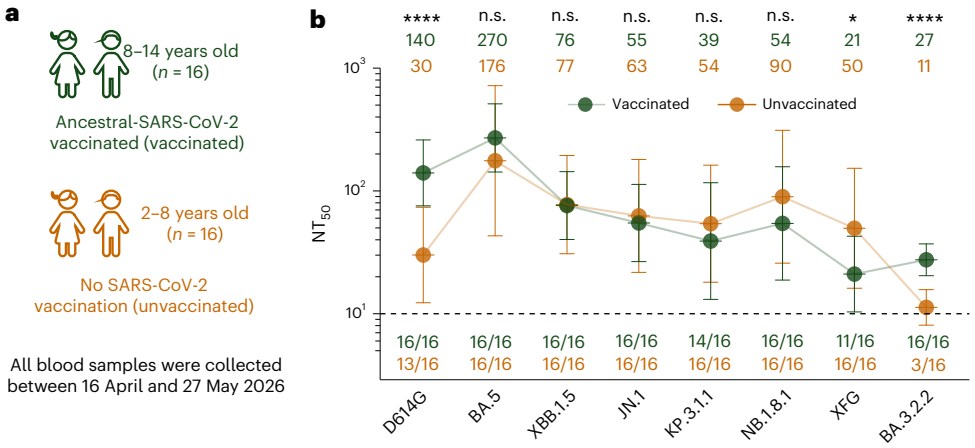


Fig. 2 | Limited BA.3.2.2 neutralization in unvaccinated children. **a**, Schematic of the vaccinated and unvaccinated paediatric cohort included in this study. **b**, Comparison of neutralizing antibody responses between the paediatric cohorts against a panel of SARS-CoV-2 pseudoviruses. Geometric mean titres (GMTs) are shown on the top. Dashed lines indicate the limit of detection (LOD, NT_{50} 10). Data are presented as GMTs, with error bars indicating geometric standard deviation. Positivity was defined as a titre above the limit of detection (NT_{50} 10) and shown under the LOD. In **a** and **b**, *n* represents the number of individual participants. Neutralization assays were conducted in at least two independent experiments. Two-sided Wilcoxon rank-sum tests were used in **b**. $^{*}P < 0.05$, $^{**}P < 0.01$, $^{***}P < 0.001$, $^{****}P < 0.0001$; n.s., not significant ($P > 0.05$).

Limited BA.3.2.2 neutralization in children

To directly investigate the immunological basis of the paediatric enrichment of BA.3.2.2, two paediatric cohorts with distinct SARS-CoV-2 vaccination histories were recruited from China, and plasma neutralization against a panel of SARS-CoV-2 variant pseudoviruses was measured (Fig. 2a and Supplementary Table 1). The first cohort consisted of unvaccinated children aged 8 years or younger ($n = 16$), representing the immune landscape of most young children, who had no exposure to the ancestral SARS-CoV-2 strain but had experienced natural Omicron infections. To serve as a comparison, the second cohort comprised children aged 8–14 years ($n = 16$) who had received priming with the inactivated Wuhan-strain vaccine. Given that China has recommended this primary vaccination for children older than 3 years since 2021, this cohort reflects the typical immune landscape of school-aged children.

Indeed, children aged 8 years or younger exhibited markedly less ancestral-strain SARS-CoV-2 immune imprinting than older children, as indicated by significantly lower neutralizing titres against D614G and overall stronger neutralization against JN.1 sublineages, notably XFG (Fig. 2b). However, the unvaccinated children cohort demonstrated significantly lower neutralizing titres against BA.3.2.2, with 13 of the 16 samples falling below the limit of detection. This diminished BA.3.2.2 neutralization was not merely a reflection of globally weaker Omicron neutralization; the vaccinated children cohort displayed robust neutralization against BA.3.2.2, exceeding their titres against XFG.

This neutralization pattern aligns with the observed paediatric enrichment of BA.3.2.2 and raises the possibility that this variant preferentially exploits antibody repertoires shaped by weaker ancestral-strain immune imprinting.

Imprinting strength dictates BA.3.2.2 neutralization

If the strength of ancestral SARS-CoV-2 immune imprinting dictates BA.3.2.2 neutralization, this phenomenon should be observable not only in unvaccinated children but also among adults with varying degrees of imprinting. Because mRNA vaccines induce strong imprinting while inactivated vaccines generate a more adaptable, Omicron-focused response following breakthrough infections[29–37], we examined a cohort of 20 adults with distinct vaccination histories. The 20 adults were long-term residents recruited from the same geographic region to reduce heterogeneity in local variant exposure (Fig. 3a and Supplementary Table 2). The cohort was stratified by vaccination history: an inactivated-only group ($n = 12$; three CoronaVac doses) and an mRNA-vaccinated group ($n = 8$; ≥1 BNT162b2 or mRNA-1273 dose), with blood sampled approximately 46 months post-initial vaccination.

Fluorescence-activated cell sorting (FACS) analysis revealed that the mRNA-vaccinated group possessed a significantly higher frequency of Wuhan-cross-reactive memory B cells than the inactivated-only group (Fig. 3b and Extended Data Figs. 3a,b). Plasma Wuhan receptor-binding domain (RBD) depletion also confirmed stronger ancestral-RBD cross-reactivity following mRNA vaccination, whereas Omicron-specific antibodies dominated the inactivated-vaccine response (Extended Data Fig. 3c). Pseudovirus neutralization assays further highlighted distinct antibody profiles between the two groups (Fig. 3c). The mRNA group's titres peaked against D614G and declined against subsequent variants, whereas the inactivated-only group displayed a flatter profile with significantly higher titres against recent variants like XFG[2,38–41]. However, BA.3.2.2 displayed the inverse pattern. BA.3.2.2 was neutralized significantly more efficiently by plasma from the mRNA-vaccinated group than by plasma from the inactivated-only group (Fig. 3c). Thus, plasma from both young children and weakly imprinted adults demonstrated selectively reduced BA.3.2.2 neutralization, thereby linking the paediatric phenotype to imprinting-associated differences in humoral immunity.

This BA.3.2.2 selective neutralization driven by imprinting level must stem from differences in the SARS-CoV-2 antigen-specific antibody repertoire landscape. To investigate this, we performed single-B-cell V(D)J sequencing of JN.1 RBD-reactive memory B cells. JN.1 RBD was selected as a common contemporary antigen at the time of sampling to capture both Omicron-specific and Wuhan–Omicron cross-reactive memory B cell responses. The strongly imprinted mRNA-vaccinated cohort was heavily enriched for immunoglobulin heavy-chain variable (IGHV) germline genes *IGHV3-53* and *IGHV3-66*, which typically encode classical 'public' Class 1 antibodies that target the ACE2-binding site[42–49] (Fig. 3d, Extended Data Figs. 4a,b and Supplementary Table 3). Such antibodies are readily elicited by ancestral-strain exposure but not Omicron infection, partly because their germline-encoded CDRH1 and CDRH2 motifs could naturally bind to the Wuhan RBD. Given their near-identical germline sequences and shared germline-encoded CDRH1/CDRH2 motifs, *IGHV3-53* and IGHV3-66 are commonly considered together as a single public Class 1 antibody family[42,47,49]. Conversely, the inactivated-only repertoire was dominated by *IGHV5-51* and *IGHV2-5* segments, which typify Omicron-specific Class 1/4 antibodies generated de novo upon antigenic shift[21]. This suggests

https://doi.org/10.1038/s41564-026-02526-w

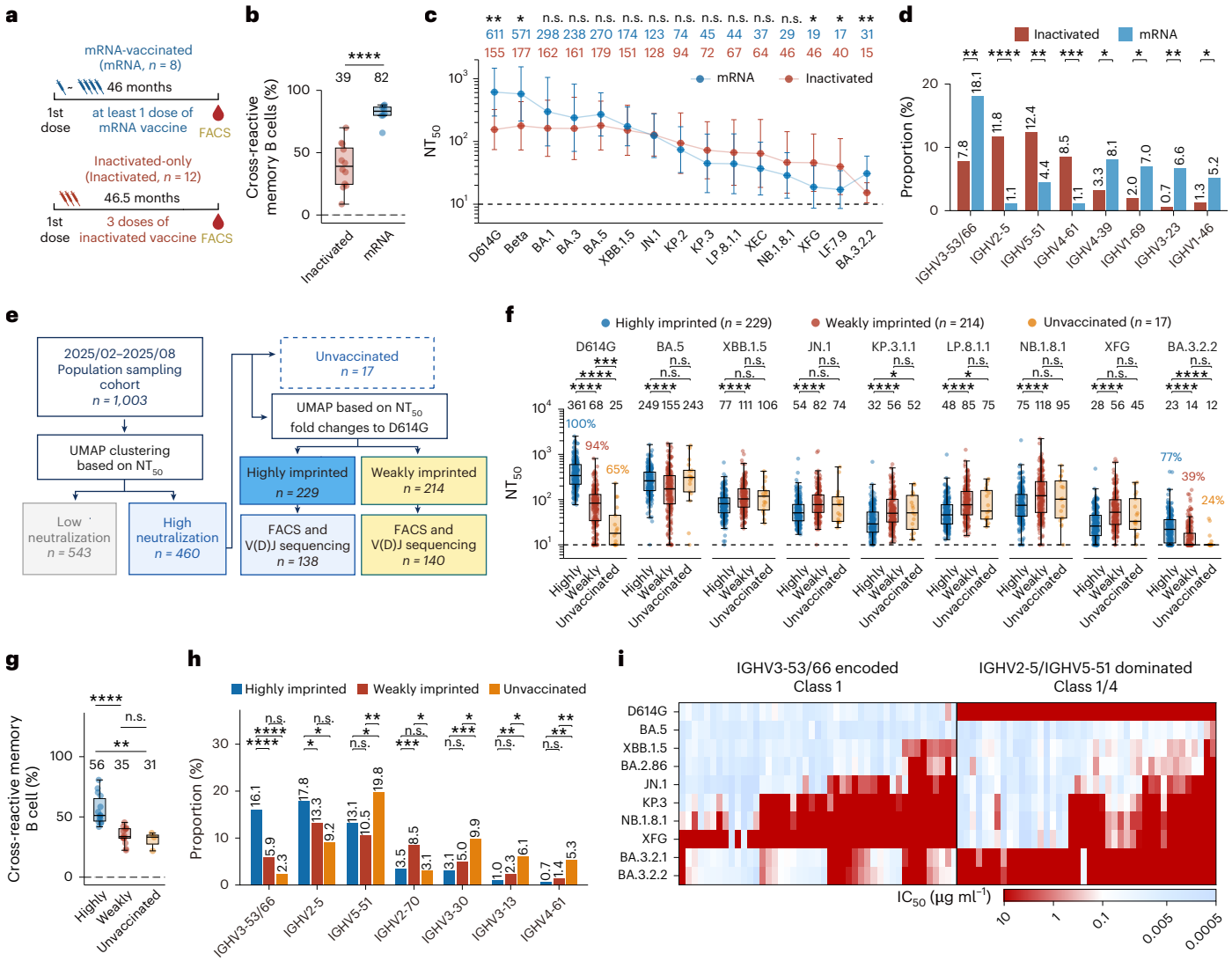


Fig. 3 | Ancestral-strain immune imprinting dictates BA.3.2.2 neutralization. **a**, Immune histories and sampling timelines of the inactivated-only and mRNA-vaccinated cohorts. **b**, Proportion of Wuhan-cross-reactive (JN.1-positive) memory B cells. **c**, Pseudovirus neutralizing antibody (NAb) responses for both cohorts. Dashed lines: limit of detection (LOD, NT_{50} 10). Error bars: geometric standard deviation. **d**, Heavy-chain V gene usage frequency among JN.1 RBD-reactive memory B cells from the mRNA-vaccinated and inactivated-only cohorts (displaying significantly different genes representing >5% of sequences in either cohort). **e**, Experimental and analysis workflow of randomly sampled human specimens. **f**, Pseudovirus NAb responses of the three groups. Dashed lines: LOD. Plasma positivity rates (NT_{50}>10) for D614G and BA.3.2.2 are noted. **g**, FACS analyses of the proportion of cross-reactive memory B cells (using a 10-in-1 sample pooling strategy). **h**, Heavy-chain V gene usage among JN.1 RBD-reactive memory B cells in highly imprinted, weakly imprinted and unvaccinated cohorts (displaying significantly different genes representing >5% in at least one cohort). **i**, Heat map of variant-escape profiles from Class 1 mAbs and Class 1/4 mAbs. Neutralization assays were conducted in at least two independent experiments. Two-sided Wilcoxon rank-sum tests were used in **b**,**c** and **f**,**g**. Two-sided Fisher's exact tests were used when any expected cell count was <5; otherwise, two-sided chi-square tests were used in **d** and **h**. $^{*}P < 0.05$, $^{**}P < 0.01$, $^{***}P < 0.001$, $^{****}P < 0.0001$; n.s., not significant ($P > 0.05$). For box plots in **b**, **f** and **g**, centre lines indicate medians; box limits indicate the 25th and 75th percentiles; whiskers extend to the smallest and largest values within 1.5× the interquartile range (IQR). For **f**, whiskers were calculated on $\log_{10}$-transformed NT_{50} values. Values above the boxes indicate means in **b** and **g** and GMTs in **f**. In **g**, *n* represents the number of independent sample pools. Otherwise, *n* represents the number of individual participants included in the corresponding cohort or analysis.

that BA.3.2.2 preferentially escapes the Omicron-specific antibodies dominant in weakly imprinted individuals while remaining sensitive to ancestral-retained Class 1 antibodies.

Although the vaccination-history cohorts identified imprinting-associated differences in BA.3.2.2 neutralization and B cell receptor (BCR) gene usage, the analysis was limited by small cohort size. To validate these imprinting-associated phenotypes in a broader population, we analysed 1,003 randomly collected blood samples (February–August 2025, Beijing and Tianjin) for downstream pseudovirus neutralization assays (Fig. 3e and Supplementary Table 2). Overall, 50% neutralization titre (NT_{50}) values against all tested SARS-CoV-2 variants increased over the sampling period in this randomly sampled cohort (Extended Data Fig. 5a,b), probably reflecting the accumulation of NB.1.8.1 exposures in the population. To minimize the influence of low-neutralization samples on later fold-change analyses and statistical comparisons, we first performed uniform manifold approximation and projection (UMAP) clustering using NT_{50} values against variants to separate the cohort into high- and low-neutralization clusters (Extended Data Fig. 6a). Among the high-neutralization samples, we excluded 17 unvaccinated individuals and then performed a second UMAP analysis based on NT_{50} fold changes of the eight variants relative to D614G. This further classified the remaining 443 samples

into highly imprinted (D614G-biased) and weakly imprinted groups (Omicron-specific) (Fig. 3f and Extended Data Fig. 6b). FACS analyses of memory B cell cross-reactivity confirmed the validity of this grouping (using a 10-in-1 sample pooling strategy), as the highly imprinted group displayed a significant enrichment of Wuhan/JN.1 cross-reactive memory B cells (Fig. 3g).

Consistent with the smaller cohorts, BA.3.2.2 exhibited stronger neutralization escape in both the weakly imprinted and unvaccinated groups compared to the highly imprinted group (Fig. 3f). Furthermore, unvaccinated individuals showed robust neutralization of most Omicron variants but markedly lower positivity against BA.3.2.2, firmly linking weak Wuhan-strain imprinting to BA.3.2.2 escape (Extended Data Fig. 7a,b). Subsequent V(D)J sequencing of JN.1-reactive memory B cells confirmed that highly imprinted individuals again possessed elevated *IGHV3-53/66* usage, whereas these gene segments were largely absent in unvaccinated individuals (Fig. 3h, Extended Data Fig. 8a and Supplementary Tables 3 and 4). Correspondingly, the ratio of *IGHV3-53/66* to *IGHV2-5* plus *IGHV5-51* usage was also higher in highly imprinted individuals (Extended Data Fig. 8b).

To definitively link these distinct antibody classes distinguished by IGHV usage to the BA.3.2.2 escape phenotype, we evaluated the neutralization profile of a panel of 87 recombinant monoclonal antibodies (mAbs) comprising 45 *IGHV3-53/66*-encoded Class 1 mAbs and 42 *IGHV2-5/IGHV5-51*-dominated Class 1/4 mAbs. As predicted, the *IGHV3-53/66*-encoded Class 1 mAbs (enriched in highly imprinted individuals) broadly retained neutralization against BA.3.2.1 and BA.3.2.2, potentially owing to their lack of key Class 1 escape substitutions, such as F456L[12]. By stark contrast, the Class 1/4 mAbs (enriched in weakly imprinted individuals) were frequently escaped, with only two retaining activity against BA.3.2.2 (Fig. 3i).

Collectively, these data provide a mechanistic explanation for the age-biased distribution of BA.3.2.2. By escaping Omicron-specific Class 1/4 antibodies while remaining sensitive to *IGHV3-53/66*-encoded Wuhan-cross-reactive Class 1 antibodies, BA.3.2.2 exploits the weakly imprinted immune landscapes typical of young children (who have lower or no ancestral-strain vaccine coverage).

Potential BA.3.2.2 evolution

The increasing prevalence of BA.3.2.2 in the paediatric population could create a large reservoir for viral replication and accelerated evolution. Similar to the evolutionary trajectory from BA.2.86 to JN.1, this could eventually enable future BA.3.2.2 sublineages to efficiently infect adult and elderly populations. To assess whether BA.3.2.2 could further expand its immune evasion after entering these weakly imprinted populations, we generated a panel of replication-incompetent BA.3.2.2 pseudoviruses carrying additional RBD substitutions. This panel included mutations observed in contemporary Class 1 antibody-evading Omicron lineages and a Y505H reversion mutant designed to test whether this specific residue drives Class 1/4 antibody escape.

Evaluating these mutants against our mAb panel revealed that most substantially escaped Class 1 antibodies, especially the 455-456 'FLip' mutation combo[50,51] (Fig. 4a). Notably, the Y505H reversion restored neutralization for the majority of Class 1/4 mAbs that parental BA.3.2.2 had completely escaped (Fig. 4b). These mAb results aligned perfectly with our plasma assays. Plasma from the highly imprinted group was significantly evaded by nearly all BA.3.2.2 mutants—often reaching escape levels comparable to XFG—indicating that additional RBD substitutions can further reduce residual BA.3.2.2 neutralizing activity (Fig. 4c). Conversely, the Y505H reversion increased plasma neutralization in the weakly imprinted and unvaccinated groups, but not in the highly imprinted group, confirming that the Y505H substitution is the key determinant of BA.3.2.2 escape from Omicron-specific antibody repertoires.

To determine whether these escape routes compromise viral fitness, we quantified receptor engagement by measuring ACE2 inhibition of these BA.3.2.2 mutant pseudoviruses and assessed spike-mediated entry using a vesicular stomatitis virus (VSV)-based pseudovirus infectivity assay in Vero cells. While some substitutions (for example, L455S) heavily impaired receptor engagement, F456L—alone or combined with L455F—maintained or slightly enhanced ACE2 binding and entry efficiency relative to parental BA.3.2.2 (Fig. 4d,e). Thus, F456L-related changes provide a plausible route by which BA.3.2.2 could acquire broader antibody escape while retaining, or potentially improving, receptor engagement and entry efficiency[52].

Discussion

The selectively reduced BA.3.2.2 neutralization observed in paediatric plasma was consistent with the preferential circulation of BA.3.2.2 in children, suggesting that emerging SARS-CoV-2 variants may exhibit population-specific susceptibility patterns. Consistent with our findings, a recent study in US cohorts similarly observed weaker BA.3.2.2 neutralization in children, while neutralization of XFG and NB.1.8.1 remained comparable across age groups[14]. Here, our findings further reveal an unusual relationship between immune imprinting, antibody-repertoire composition and this age-biased distribution of BA.3.2.2. Whereas strong ancestral-strain imprinting generally constrains adaptation to recent Omicron variants (for example, NB.1.8.1 and XFG), BA.3.2.2 exhibits the opposite pattern. It preferentially escapes the Omicron-specific Class 1/4 antibodies enriched in weakly imprinted individuals, while remaining sensitive to the *IGHV3-53/66*-encoded, Wuhan-cross-reactive Class 1 antibodies enriched in strongly imprinted individuals. This antibody-class specificity mechanistically explains the paediatric enrichment of BA.3.2.2, given that children generally have lower ancestral-strain vaccine coverage and correspondingly weaker Wuhan-strain imprinting. In China, the large and growing population with weakly imprinted immune histories may likewise create a more permissive landscape for future BA.3.2.2 expansion. Its current limited detection may be partly due to limited sequence deposition and the sustained predominance of the earlier-established NB.1.8.1 lineage.

A critical insight derived from these observations is that classic immune imprinting does not act as a uniform barrier to neutralizing efficacy; rather, its utility is highly dependent on the precise conformation of the emerging variant's antigenic landscape. While imprinting has historically been characterized as a constraint that leaves populations vulnerable to incremental drift, it serves here as a robust protective shield against specific saltation variants. This is due to the broad-spectrum neutralization of germline-encoded Class 1 public antibodies, which the virus has yet to successfully bypass. By contrast, the de novo, Omicron-specific responses that dominate the weakly imprinted populations are highly specialized but narrow, rendering them vulnerable to BA.3.2.2.

This points to a substantial public health vulnerability. Paediatric cohorts, lacking ancestral-strain exposures, provide an immunological niche—an incubator—where BA.3.2.2 can propagate with minimal resistance. Within this weakly imprinted population, the genetic barrier for the virus to acquire supplementary mutations (such as F456L-related changes) is extremely low. This raises a concern: sustained transmission of BA.3.2.2 in paediatric populations may catalyse the emergence of secondary variants that combine the paediatric antibody-response-evading features of BA.3.2.2 with Class 1 mutations that evade adult antibody responses. Such evolutionary trajectories would allow the lineage to breach the imprinted immunity of the adult population, potentially driving widespread global transmission. Notably, JN.1-updated mRNA vaccination only modestly improves BA.3.2.2 neutralization relative to other variants[12], and if this gain is substantially mediated by Wuhan-cross-reactive Class 1 antibodies, such protection could remain particularly vulnerable to additional Class 1 escape mutations.

Thus, the impact of immune imprinting depends heavily on how viral antigenic change intersects with stratified population-level

https://doi.org/10.1038/s41564-026-02526-w

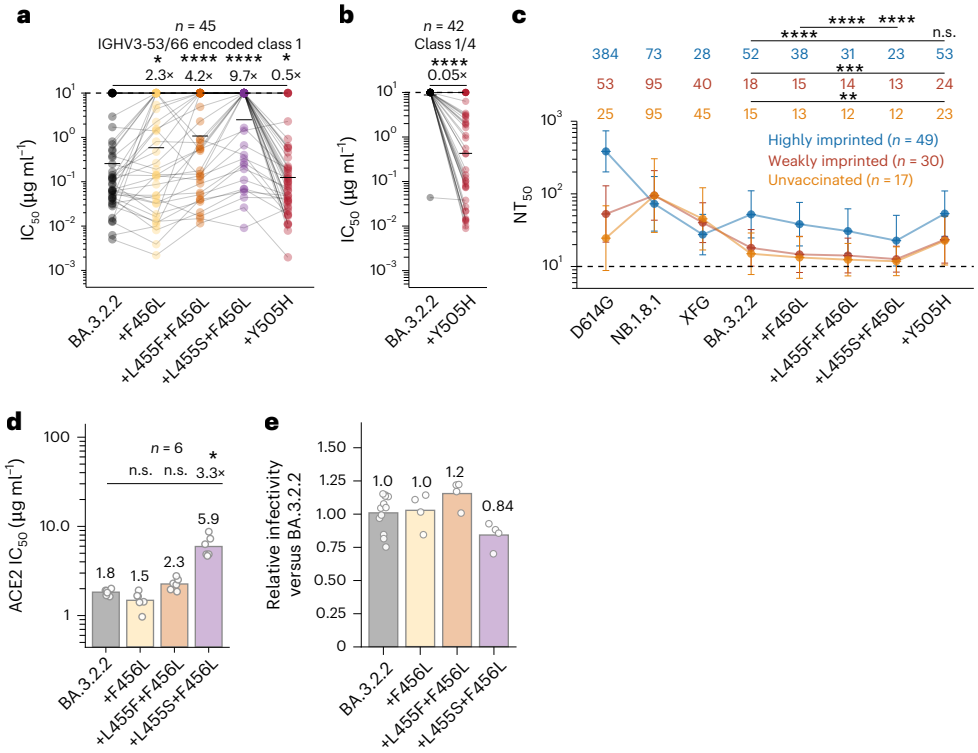


Fig. 4 | RBD substitutions enable further escape of BA.3.2.2 from strongly imprinted immunity. a, Scatter-line plot showing escape profiles of different BA.3.2.2 mutants from Class 1 mAbs encoded by *IGHV3-53/66*. **b**, Neutralization recovery of Class 1/4 mAbs dominated by *IGHV2-5* and *IGHV5-51* by Y505H reverse mutation. In **a** and **b**: points represent individual mAbs, lines connect measurements from the same mAb, and horizontal black bars indicate geometric mean IC_{50} values. **c**, NAb response of the randomly selected plasma from BA.3.2.2-positive highly imprinted, weakly imprinted and unvaccinated individuals against a panel of BA.3.2.2 mutant pseudoviruses. Dashed lines indicate the LOD (NT_{50} 10). Data are presented as geometric mean titres (GMTs), with error bars indicating geometric standard deviation. In total, 49 BA.3.2.2-neutralizing plasma samples from the highly imprinted group, 30 samples from the weakly imprinted group, and all 17 samples from the unvaccinated group are randomly selected. **d**, ACE2 IC_{50} against a panel of BA.3.2.2 mutant pseudoviruses. Bars indicate geometric mean values. **e**, Relative infectivity of BA.3.2.2 mutants in Vero cells. Infectivity was assessed by use of vesicular stomatitis virus pseudoviruses. Bars indicate mean values. In **a** and **b**, *n* represents the number of individual mAbs; in **c**, *n* represents the number of individual participants; in **d**, *n* represents the number of independent biological replicates of the ACE2 inhibition assay; in **e**, each point represents a technical replicate. All assays were conducted in at least two independent experiments. Two-sided Wilcoxon signed-rank tests were used in **a**–**d**. $^{*}P < 0.05$, $^{**}P < 0.01$, $^{***}P < 0.001$, $^{****}P < 0.0001$; n.s., not significant ($P > 0.05$).

antibody repertoires. These findings underscore that future paediatric SARS-CoV-2 vaccination campaigns should weigh the immediate benefits of variant-matched antigens against the long-term utility of establishing a broad antibody baseline. There is a critical need for immunization strategies that combine variant-matched specificity with the breadth conferred by ancestral-induced Class 1 neutralizing antibodies to ensure balanced protection across all age groups.

Methods

Ethics statement

All research involving human participants complied with relevant ethical regulations. The research protocol and the collection of human blood samples for all cohorts were approved by the relevant institutional review boards or ethics committees. The paediatric cohort was approved by the Institutional Review Board of Shenzhen Luohu People's Hospital (ethics approval no. 2260206006) and the Ethics Committee of Beijing Children's Hospital, Capital Medical University (IEC-C-006-A04-V.08). The population sampling cohort was approved by the Ethics Committee of Tianjin First Central Hospital (KEYAN20241022-2) and the Institutional Review Board of Beijing Ditan Hospital, Capital Medical University (DTEC-KY2024-112-01). The mRNA-vaccinated cohort was approved by the Institutional Review Board of Shenzhen Institutes of Advanced Technology, Chinese Academy of Sciences (SIAT-IRB-230715-H0667), and the inactivated-vaccine cohort was approved by the Institutional Review Board of Beijing Ditan Hospital, Capital Medical University (DTEC-KY2024-112-01). The population-sampling cohort was collected specifically for this study and was not part of routine clinical care. All participants provided their agreement for the collection, storage and use of their blood samples strictly for research purposes and the subsequent publication of related data. Written informed consent was obtained from all adult participants. For participants who were minors, written informed consent was obtained from their parents or legal guardians. All participants received compensation for participation. Participant age, sex and cohort size are detailed in Supplementary Tables 1 and 2.

Cell culture

All cell lines were obtained from the indicated commercial repositories or manufacturers. No additional authentication was performed in our laboratory. Cell lines were not tested for mycoplasma contamination.

Human plasma and PBMC isolation

Blood samples were obtained from participants with different SARS-CoV-2 vaccination histories (detailed in Supplementary Tables 1 and 2). To isolate plasma and peripheral blood mononuclear cells (PBMCs), whole blood was diluted 1:1 with phosphate-buffered saline (PBS) (Invitrogen, C10010500BT) containing 2% (v/v) fetal bovine serum (FBS; Hyclone, SH30406.05) and separated by density gradient centrifugation using Ficoll (Cytiva, 17-1440-03). The upper plasma layer was collected, aliquoted and stored at or below −20 °C. Before use in assays, plasma samples were heat-inactivated at 56 °C for 30 min and assessed for neutralizing titres against SARS-CoV-2 variant spike-pseudotyped VSV.

The PBMC layer was collected from the interface and processed further. Following red blood cell lysis (Invitrogen eBioscience 1× RBC Lysis Buffer, 00-4333-57) and washing, PBMCs were either used immediately or cryopreserved in FBS with 10% (v/v) dimethyl sulfoxide (Solarbio, D8371) for storage in liquid nitrogen. All PBMC samples were transported on dry ice. For B cell isolation, cryopreserved PBMCs were thawed in PBS supplemented with 5% (v/v) FBS. B cells were subsequently enriched by immunomagnetic positive selection using the EasySep Human CD19 Positive Selection Kit II (STEMCELL, 17854) following the manufacturer's protocol. The resulting purified B cells were resuspended in PBS with 2% (v/v) FBS, and cell counts and viability were determined using 0.4% (w/v) trypan blue staining (Invitrogen, T10282) on a Countess Automated Cell Counter (Invitrogen).

Pseudovirus preparation and neutralization assay

We generated SARS-CoV-2 variant spike protein pseudovirus as described previously[3,21,23,53–55]. Plasmids encoding a codon-optimized SARS-CoV-2 Spike (S) protein were constructed by inserting the S gene into the pcDNA3.1 vector. To produce pseudovirus, 293T cells (ATCC, CRL-3216) were transfected with the Spike-expressing plasmids with Lipofectamine 3000 (Invitrogen, L3000015) and subsequently infected with G*ΔG-VSV (Kerafast, EH1020-PM). After 24 h, the supernatant containing the pseudovirus was harvested, filtered through a 0.45-μm filter (Millipore), aliquoted and stored at −80 °C.

Neutralization assays were performed using the Huh-7 cell line (JCRB, 0403). mAbs or plasma samples were serially diluted in DMEM (Hyclone, SH30243.01) and incubated with the pseudovirus in 96-well plates for 1 h at 37 °C with 5% CO_2. Following incubation, Huh-7 cells were seeded into the wells (2×10^4 cells per well) and cultured for an additional 24 h at 37 °C with 5% CO_2. To assess infection levels, the culture supernatant was removed, and 50 μl was left in each well. The Bright-Lite Luciferase Assay Substrate was reconstituted with its corresponding Assay Buffer (Vazyme, DD1209-03-AB), and this mixture was added to the wells. After incubating in the dark for 2 min, luminescence was measured using a microplate spectrophotometer (PerkinElmer, HH3400). For ACE2 inhibition assays, serially diluted recombinant human ACE2-Fc was used in place of mAbs, and the assay was otherwise performed under the same conditions described above. The NT_{50} or half-maximal inhibitory concentration (IC_{50}) values were determined using a three-parameter logistic regression model.

Pseudovirus-based infectivity assay

Vero E6 cells (ATCC CRL-1586) were trypsinized and co-incubated with pseudoviruses carrying BA.3.2.2 mutations in 96-well plates (2×10^4 cells per well) to permit viral adsorption and entry. After incubation for 24 h at 37 °C with 5% CO_2, the supernatant was removed, leaving 50 μl per well. Bright-Lite Luciferase Assay Substrate, reconstituted with Assay Buffer (Vazyme, DD1209-03-AB), was added, and luminescence was measured after 2 min in the dark using a microplate spectrophotometer (PerkinElmer, HH3400).

Flow cytometry analysis and antigen-specific B cell sorting

For the isolation of antigen-specific human B cells, enriched B cell populations from PBMCs were prepared for FACS. Cells were resuspended in PBS containing 2% (v/v) FBS and 1 mM EDTA, and were stained in a total volume of 100 μl per reaction. Cells were incubated with 2.5 μl Human TruStain FcX (BioLegend, 422302) per reaction for 10 min on ice in the dark first. The staining panel comprised 3 μl FITC anti-human CD20 (BioLegend, 302304), 3 μl Brilliant Violet 605 anti-human CD27 (BioLegend, 302830), 2 μl PE/Cyanine7 anti-human IgM (BioLegend, 314532) and 2 μl PE/Cyanine7 anti-human IgD (BioLegend, 348210) per reaction. Antigen-specific cells were detected using biotinylated JN.1 RBD (Sino Biological, 40592-V49H16-B) conjugated with PE-streptavidin (BioLegend, 405204) and APC-streptavidin (BioLegend, 405207), and Wuhan RBD (Sino Biological, 40592-V27H-B) conjugated with BV421-streptavidin (BioLegend, 405225). The viability dye 7-AAD (Invitrogen, 00-6993-50) was used to exclude dead cells. A gating strategy was applied to sort single, viable (7-AAD$^-$), class-switched (IgM$^-$ and IgD$^-$), CD20$^+$CD27$^+$ memory B cells that were positive for JN.1 RBD. Data were collected via Summit 6.0 software (Beckman Coulter). Data from all experiments were uniformly analysed using FlowJo v10.8 (BD Biosciences).

Single-cell V(D)J sequencing

For the 10x Genomics workflow, sorted antigen-specific B cells, suspended in PBS with 10% (v/v) FBS, were processed with the Chromium Next GEM Single Cell V(D)J Reagent Kits v2 (10x Genomics, CG000331). The cell suspension was loaded onto a 10x Chromium Controller to generate gel beads-in-emulsion, which facilitate the barcoding of mRNA and subsequent reverse transcription within individual droplets. Following cDNA synthesis, the product was purified using a SPRIselect Reagent Kit (Beckman Coulter, B23318) and pre-amplified. Targeted enrichment of paired V(D)J sequences was then achieved using 10x-specific BCR primers, and the resulting products were used for sequencing library construction. These final libraries were sequenced on an Illumina NovaSeq 6000 platform with a NovaSeq 6000 S4 Reagent Kit v1.5 (300 cycles; Illumina, 20028312). The 10x Genomics V(D)J Illumina sequencing data were assembled as BCR contigs and aligned to the B cell V(D)J reference using Cell Ranger (v.6.1.1) pipeline. For human-source *IGH*, *IGL* and *IGK* contigs, we used GRCh38 as reference. Only the productive contigs and B cells with one heavy chain and one light chain were kept to remove doublets. The germline V(D)J genes were identified and annotated using IgBlast (v1.17.1)[56].

For the plate-based method, single antigen-specific B cells were sorted directly into the individual wells of 96-well plates, each containing 4 μl of lysis buffer (0.095% Triton X-100, 2.5 μM oligo-dT primer: 5′-AAGCAGTGGTATCAACGCAGAGTACTTTTTTTTTT TTTTTTTTTTTTTTTTTTTTVN-3′, 2.5 mM deoxynucleoside triphosphates and 1 U μl^{-1} RNase inhibitor). The plates were immediately processed by vortexing, centrifugation and incubation at 72 °C for 3 min to denature RNA secondary structures, followed by rapid chilling on ice. Reverse transcription (RT) was performed in each well by adding 5.7 μl of an RT master mix (final concentrations: 1× HiScript III first-strand buffer, 10 U μl^{-1} HiScript III reverse transcriptase, 2 U μl^{-1} RNase inhibitor, 5 mM dithiothreitol, 1 M betaine, 6 mM $MgCl_2$, 1 μM template-switching oligonucleotide primer: 5′-AAGCAGTGGTATCAACGCAGAGTACATrGr G+G-3′). The RT reaction was incubated at 37 °C for 60 min, followed by enzyme inactivation at 85 °C for 5 s. The resulting cDNA served as a template for amplifying full-length immunoglobulin heavy- and light-chain V(D)J sequences via a two-round nested PCR strategy using Phanta Max Master Mix (Vazyme, P515). The first PCR round used a multiplex primer pool targeting all VH, Vκ and Vλ gene families, along with constant region-specific reverse primers. A second, nested PCR round was then performed with internal primers to enhance specificity and yield. Sequences of the primers used for plate-based single-B-cell BCR amplification are provided in Supplementary Table 3. Final amplicons were purified and subsequently analysed by Sanger sequencing. The germline V(D)J genes were identified and annotated using IgBlast (v1.22.0)[56].

mAb expression and purification

The sequences for the antibody heavy and light chains were initially codon-optimized for expression in human cells (GenScript). The variable regions (VH and VL) were then separately inserted into corresponding expression vectors (pCMV3-CH, pCMV3-CL or pCMV3-CK). Plasmids of the heavy and light chain constructs were transformed into *Escherichia coli* DH5α competent cells (Tsingke, TSC-C01-96). After overnight incubation at 37 °C, single colonies were picked for colony PCR identification. Plasmid DNA of expanded cultures was extracted (CWBIO, CW2105) and verified by Sanger sequencing.

For protein production, heavy- and light-chain plasmids were cotransfected into Expi293F cells (Thermo Fisher, A14527) using polyethylenimine (Yeasen, 40816ES03). The plasmid–polyethylenimine complexes were prepared in sterile 0.9% NaCl solution before being added to the cell culture. The transfected cells were cultured at 36.5 °C with 5% CO_2 and 175 rpm shaking for 6–10 days. A nutrient supplement (OPM Biosciences, F081918-001) was added to each culture at 24 h post-transfection and every 48 h thereafter.

To purify the antibodies, the culture supernatant was first clarified by centrifugation (3,000*g*, 10 min). The supernatant was then incubated with Protein A magnetic beads (GenScript, L00695) for 2 h to allow antibody binding. The beads were subsequently washed, and the bound antibodies were eluted using a KingFisher automated purification system (Thermo Fisher). The concentration of the purified antibody was determined using a NanoDrop spectrophotometer (Thermo Fisher, 840-317400), and its purity was assessed by SDS–PAGE (LabLead, P42015).

RBD depletion of plasma

To deplete RBD-specific antibodies from plasma, 50 µl of Dynabeads MyOne Streptavidin T1 (Invitrogen, 65601) were washed once with PBS. Ten micrograms of biotinylated SARS-CoV-2 Wuhan RBD was incubated with the washed beads for 1 h with gentle rotation to allow binding via streptavidin–biotin interaction. The beads were then collected using a magnetic rack for 2–3 min, the supernatant was discarded, and the beads were washed three times with PBS to remove unbound proteins. Subsequently, 200–400 µl of plasma was incubated with the RBD-conjugated beads for 1 h with gentle rotation to allow specific antibody binding. Finally, the tubes were placed on the magnetic rack, and the supernatant representing the RBD-depleted plasma was carefully collected for downstream analyses.

Enzyme-linked immunosorbent assays

High-binding 96-well plates (NEST, 504201) were coated overnight at 4 °C with SARS-CoV-2 Wuhan (Sino Biological, 40592-V27H-B) or JN.1 RBD proteins (Sino Biological, 40592-V49H16-B). The following day, plates were washed three times with 1× PBS containing Tween-20 (PBST, Solarbio, P1033) and blocked with 250 µl 5% bovine serum albumin (Solarbio, A8020) in 1× PBST for 2 h at 37 °C to prevent non-specific binding. After three additional washes, 100 µl of serially diluted antibodies or plasma samples were added to the wells and incubated for 30 min at room temperature. Unbound antibodies were removed by five washes with 1× PBST. Subsequently, 100 µl of HRP-conjugated goat anti-mouse IgG (H + L) cross-adsorbed secondary antibody (Invitrogen, G21040) or peroxidase AffiniPure goat anti-human IgG (H + L) (Jackson Immunoresearch, 109-035-003) was added and incubated for 30 min at room temperature. Following a final five washes, the signal was developed by adding 100 µl of TMB substrate (Solarbio, PR1200) to each well and incubating for 8 min in the dark. The reaction was terminated by adding 50 µl of stop solution (Solarbio, C1058). The optical density (OD) was measured at 450 nm with a reference wavelength of 630 nm using a Multiskan FC microplate reader (Thermo Scientific). Final absorbance values were obtained by subtracting the OD_{630} reading from the OD_{450} reading for each well.

GISAID sequence retrieval and metadata curation

SARS-CoV-2 metadata records with collection dates from 1 December 2025 through 24 May 2026 were retrieved from the GISAID EpiCoV database in five date-partitioned exports. The exported batches were merged and deduplicated by accession ID before analysis. Records assigned to BA.3.2.2*, XFG* or NB.1.8.1* were retained, where the asterisk denotes the parental Pango lineage and all designated descendants. Lineage assignments in the GISAID metadata were matched against lineage_notes.txt and alias_key.json obtained from the cov-lineages/pango-designation repository; aliased lineage names were expanded to identify descendants of each target lineage. Records with missing or non-informative collection date, location, patient age or lineage information were excluded. Country was extracted from the country component of the GISAID location field. Ages reported in days, weeks or months were assigned an age of 0 years, decimal ages were converted to integer years, and unparseable or clearly erroneous values were excluded. Exact ages and age ranges that could be assigned unambiguously were classified into 0–9, 10–17, 18–29, 30–39, 40–49, 50–59, 60–69, 70–79, 80–89 and ≥90-year groups. Broad age intervals crossing these boundaries were excluded from age-distribution analyses. France was excluded from the age-distribution analyses shown in Fig. 1b,c and Extended Data Fig. 1 because a large proportion of French records reported patient age only as broad intervals that crossed the prespecified age-group boundaries.

Age-stratified vaccination coverage data

Age-stratified COVID-19 vaccination data were obtained from official public health surveillance sources, including the European Centre for Disease Prevention and Control for European Union/European Economic Area countries, the US Centers for Disease Control and Prevention for the USA, and the Government of Canada COVID-19 vaccination coverage database for Canada. Coverage was defined as the proportion of individuals who had received at least one vaccine dose and was analysed retrospectively over the period of primary ancestral-strain vaccination campaigns. For the harmonized comparison shown in Fig. 1d, national-level records were retained and source-specific age strata were mapped to the prespecified age categories used for descriptive comparison. Age groups that overlapped, crossed category boundaries or could not be assigned unambiguously to a single harmonized stratum, such as broad categories covering individuals aged <60 years or 18–69 years, were excluded to avoid double counting or arbitrary allocation. Records were aligned to a common weekly time scale. For European Union/European Economic Area countries, cumulative first-dose counts were reconstructed from weekly first-dose reports and divided by the corresponding age-specific population denominators. For the USA, the latest national cumulative observation within each week was retained, and missing cumulative counts were reconstructed from the reported coverage and census denominator where possible. For Canada, analyses were restricted to national records for all sexes; because an explicit population denominator was unavailable, age-specific denominators were estimated from the ratio of cumulative first-dose counts to reported coverage and summarized across reporting weeks. The harmonized coverage estimates were aggregated across contributing countries using population weighting, calculated as the sum of cumulative first-dose counts divided by the sum of the corresponding age-specific population denominators. Countries contributed to an age stratum from their first available report, after which cumulative values were carried forward across subsequent weeks. In Extended Data Fig. 2, country-specific vaccination trajectories are additionally presented using the original age categories reported by each surveillance source, without harmonization-based exclusion, to provide a more detailed view of vaccine uptake across the full set of available age strata.

Statistics and reproducibility

No statistical methods were used to predetermine sample sizes, but our sample sizes are similar to those reported in previous publications[21,29,30]. Normality and homogeneity of variance were not formally tested. Continuous variables were analysed using non-parametric Wilcoxon tests, which do not assume normality, whereas categorical data were analysed using Fisher's exact tests or chi-square tests, for which assumptions of normality and homogeneity of variance are not applicable. Fisher's exact tests were used when any expected cell count was <5; otherwise, chi-square tests were used. As this was an observational study, participants were not randomized to experimental groups, and no additional

randomization or blocking was applied during sample processing or experimental assays. Investigators performing the experimental assays were not blinded to participant group information during data collection; statistical analyses were not performed blind to group allocation.

Reporting summary

Further information on research design is available in the Nature Portfolio Reporting Summary linked to this article.

Data availability

Information on individuals providing blood samples and neutralization titres involved in this study has been included in Supplementary Tables 1 and 2. The paired BCR sequences generated by plate-based single B cell sequencing from human samples and the primers used are provided in Supplementary Table 3. The processed productive amino acid sequences obtained from the 10x Genomics single-cell V(D)J sequencing data are provided in Supplementary Table 4. The raw 10x Genomics single-cell V(D)J sequencing reads generated in this study have been deposited in the CNGB Sequence Archive (CNSA) under accession number CNP0009821 and in the Genome Sequence Archive for Human (GSA-Human) at the National Genomics Data Center, China National Center for Bioinformation, under accession number HRA020962 (BioProject: PRJCA073984). Requests for resources and reagents should be directed to and will be fulfilled by the lead contact, Y.C., and are subject to a Material and Data Transfer Agreement. All enquiries will be replied to within 1 week. Source data are provided with this paper.

Code availability

No custom algorithms or software were developed. Data analysis and visualization was performed using standard software or packages/libraries in R v4.3.2 or python v3.10.11, including tidyverse v2.0.0[57], ggplot2 v3.5.1[58] and umap v0.2.10.0[59] in R and NumPy v1.26.4[60], Matplotlib v3.8.4[61] and SciPy v1.13.0[62] in Python.

References

1. Korber, B., Fischer, W. & Theiler, J. Real-time monitoring of SARS-CoV-2 evolution during the COVID-19 pandemic. *Cell Host Microbe* **33**, 1802–1806 (2025).
2. Mellis, I. A. et al. Antibody evasion and receptor binding of SARS-CoV-2 LP.8.1.1, NB.1.8.1, XFG, and related subvariants. *Cell Rep.* **44**, 116440 (2025).
3. Guo, C. et al. Antigenic and virological characteristics of SARS-CoV-2 variants BA.3.2, XFG, and NB.1.8.1. *Lancet Infect. Dis.* **25**, e374–e377 (2025).
4. Uriu, K. et al. Virological characteristics of the SARS-CoV-2 NB.1.8.1 variant. *Lancet Infect. Dis.* **25**, e443 (2025).
5. Cao, G., Xu, C., Wang, L., Chai, K. & Wu, B. Global surveillance and biological characterization of the SARS-CoV-2 NB.1.8.1 variant: an emerging VUM lineage under scrutiny. *Viruses* **17**, 1457 (2025).
6. Kaku, Y. et al. Humoral immunity after LP.8.1 monovalent vaccines against a broad range of SARS-CoV-2 variants including XEC, LP.8.1, NB.1.8.1, XFG, and BA.3.2. *Lancet Infect. Dis.* **26**, e142–e143 (2026).
7. Azhar, L. E., Samkari, D. A., Hassan, A. M., Alsayed, S. M. & Azhar, E. I. The emergence and characterization of SARS-CoV-2 variant XFG ("Stratus"): comparative virological, epidemiological, and public-health perspectives. *J. Epidemiol. Glob. Health* **16**, 8 (2026).
8. Li, P., Zheng, Y.-M. & Liu, S.-L. Altered infectivity, cell–cell fusion, and immune evasion of SARS-CoV-2 BA.3.2 and LP.8.1 variants. *J. Virol.* **100**, e00016–26 (2026).
9. Happle, C. et al. Effects of LP.8.1-adapted mRNA vaccination on SARS-CoV-2 variant neutralisation. *Lancet Infect. Dis.* **26**, e3–e5 (2026).
10. Dor, G. et al. Identification and genomic characterization of BA.3.2: a highly divergent BA.3-related SARS-CoV-2 lineage from southern Africa. *Virus Evol* **12**, veag016 (2026).
11. Turner, S. A. et al. Antigenic characterization of SARS-CoV-2 variants BA.3.2.1 and BA.3.2.2 in three animal models. Preprint at *bioRxiv* https://doi.org/10.64898/2026.05.24.727525 (2026).
12. Miyakawa, K. et al. Cross-neutralization of SARS-CoV-2 BA.3.2.2 lineage by JN.1 mRNA vaccine-induced immunity. *Int. J. Infect. Dis.* **170**, 108954 (2026).
13. Shakya, M. et al. Early detection and surveillance of the SARS-CoV-2 variant BA.3.2 — worldwide, November 2024–February 2026. *MMWR Morb. Mortal. Wkly Rep.* **75**, 130–137 (2026).
14. Wu, M. et al. S ARS-CoV-2 BA.3.2.2 is more evasive of neutralisation by plasma from young children. *Lancet Infect. Dis.* **26**, e328–e329 (2026).
15. Zhang, L. et al. Epidemiological and virological update on the emerging SARS-CoV-2 variant BA.3.2. *Lancet Infect. Dis.* **26**, e1–e2 (2026).
16. Nasir, A. et al. Predictive modeling of immune escape and antigenic grouping of SARS-CoV-2 variants. *J. Virol.* **100**, e00225–26 (2026).
17. Zhang, L., Hoffmann, M. & Pöhlmann, S. Does BA.3.2 epidemiology imply a change in SARS-CoV-2 evolution? *Lancet Infect. Dis.* **26**, 555–557 (2026).
18. Leslie, D. K. et al. PS-09 - investigation into possible increased susceptibility to the COVID-19 BA.3.2 variant in children. *J. Public Health* **48**, i31 (2026).
19. Davies, N. G. et al. Age-dependent effects in the transmission and control of COVID-19 epidemics. *Nat. Med.* **26**, 1205–1211 (2020).
20. Viner, R. M. et al. Susceptibility to SARS-CoV-2 infection among children and adolescents compared with adults: a systematic review and meta-analysis. *JAMA Pediatr.* **175**, 143–156 (2021).
21. Jian, F. et al. Evolving antibody response to SARS-CoV-2 antigenic shift from XBB to JN.1. *Nature* **637**, 921–929 (2025).
22. Yisimayi, A. et al. Prolonged Omicron-specific B cell maturation alleviates immune imprinting induced by SARS-CoV-2 inactivated vaccine. *Emerg. Microbes Infect.* **13**, 2412623 (2024).
23. Yisimayi, A. et al. Repeated Omicron exposures override ancestral SARS-CoV-2 immune imprinting. *Nature* **625**, 148–156 (2024).
24. You, L. et al. Multiple infections with Omicron variants increase breadth and potency of Omicron-specific neutralizing antibodies. *Cell Discov.* **11**, 49 (2025).
25. Gao, B. et al. Repeated vaccination of inactivated SARS-CoV-2 vaccine dampens neutralizing antibodies against Omicron variants in breakthrough infection. *Cell Res.* **33**, 258–261 (2023).
26. Faraone, J. N. & Liu, S.-L. Immune imprinting as a barrier to effective COVID-19 vaccines. *Cell Rep. Med.* **4**, 101291 (2023).
27. Kotaki, R. et al. Repeated Omicron exposures redirect SARS-CoV-2–specific memory B cell evolution toward the latest variants. *Sci. Transl. Med.* **16**, eadp9927 (2024).
28. Abdullahi, A. et al. SARS-CoV-2 Omicron infection reveals imprinted antibody responses in the absence of vaccination. *iScience* **29**, 115910 (2026).
29. Liang, C.-Y. et al. Imprinting of serum neutralizing antibodies by Wuhan-1 mRNA vaccines. *Nature* **630**, 950–960 (2024).
30. Tortorici, M. A. et al. Persistent immune imprinting occurs after vaccination with the COVID-19 XBB.1.5 mRNA booster in humans. *Immunity* **57**, 904–911.e4 (2024).
31. Wang, Q. et al. Deep immunological imprinting due to the ancestral spike in the current bivalent COVID-19 vaccine. *Cell Rep. Med.* **4**, 101258 (2023).
32. Reynolds, C. J. et al. Immune boosting by B.1.1.529 (Omicron) depends on previous SARS-CoV-2 exposure. *Science* **377**, eabq1841 (2022).

33. Chemaitelly, H. et al. Long-term COVID-19 booster effectiveness by infection history and clinical vulnerability and immune imprinting: a retrospective population-based cohort study. *Lancet Infect. Dis.* **23**, 816–827 (2023).
34. Wang, Z. et al. Memory B cell responses to Omicron subvariants after SARS-CoV-2 mRNA breakthrough infection in humans. *J. Exp. Med.* **219**, e20221006 (2022).
35. Wang, Q. et al. XBB.1.5 monovalent mRNA vaccine booster elicits robust neutralizing antibodies against XBB subvariants and JN.1. *Cell Host Microbe* **32**, 315–321.e3 (2024).
36. Johnston, T. S. et al. Immunological imprinting shapes the specificity of human antibody responses against SARS-CoV-2 variants. *Immunity* **57**, 912–925.e4 (2024).
37. Addetia, A. et al. Neutralization, effector function and immune imprinting of Omicron variants. *Nature* **621**, 592–601 (2023).
38. Wang, Q. et al. Antibody evasiveness of SARS-CoV-2 subvariants KP.3.1.1 and XEC. *Cell Rep.* **44**, 115543 (2025).
39. Li, P. et al. Neutralization and spike stability of JN.1-derived LB.1, KP.2.3, KP.3, and KP.3.1.1 subvariants. *mBio* **16**, e00464-25 (2025).
40. Li, P. et al. Neutralization escape, infectivity, and membrane fusion of JN.1-derived SARS-CoV-2 SLip, FLiRT, and KP.2 variants. *Cell Rep.* **43**, 114520 (2024).
41. Wang, Q. et al. Robust SARS-CoV-2-neutralizing antibodies sustained through 6 months post XBB.1.5 mRNA vaccine booster. *Cell Rep. Med.* **5**, 101701 (2024).
42. Yuan, M. et al. Structural basis of a shared antibody response to SARS-CoV-2. *Science* **369**, 1119–1123 (2020).
43. Wang, Y. et al. A large-scale systematic survey reveals recurring molecular features of public antibody responses to SARS-CoV-2. *Immunity* **55**, 1105–1117.e4 (2022).
44. Li, L. et al. Breakthrough infection elicits hypermutated IGHV3-53/3-66 public antibodies with broad and potent neutralizing activity against SARS-CoV-2 variants including the emerging EG.5 lineages. *PLoS Pathog.* **19**, e1011856 (2023).
45. Vanshylla, K. et al. Discovery of ultrapotent broadly neutralizing antibodies from SARS-CoV-2 elite neutralizers. *Cell Host Microbe* **30**, 69–82 (2022).
46. Yan, Q. et al. Germline IGHV3-53-encoded RBD-targeting neutralizing antibodies are commonly present in the antibody repertoires of COVID-19 patients. *Emerg. Microbes Infect.* **10**, 1097–1111 (2021).
47. Zhang, Q. et al. Potent and protective IGHV3-53/3-66 public antibodies and their shared escape mutant on the spike of SARS-CoV-2. *Nat. Commun.* **12**, 4210 (2021).
48. Nutalai, R. et al. Potent cross-reactive antibodies following Omicron breakthrough in vaccinees. *Cell* **185**, 2116–2131 (2022).
49. Tan, T. J. C. et al. Sequence signatures of two public antibody clonotypes that bind SARS-CoV-2 receptor binding domain. *Nat. Commun.* **12**, 3815 (2021).
50. Qu, P. et al. Immune evasion, infectivity, and fusogenicity of SARS-CoV-2 BA.2.86 and FLip variants. *Cell* **187**, 585–595.e6 (2024).
51. Jian, F. et al. Convergent evolution of SARS-CoV-2 XBB lineages on receptor-binding domain 455–456 synergistically enhances antibody evasion and ACE2 binding. *PLoS Pathog.* **19**, e1011868 (2023).
52. Zhang, L. et al. Host cell entry and neutralisation sensitivity of SARS-CoV-2 BA.3.2. *Lancet Microbe* **6**, 101165 (2025).
53. Liu, J. et al. Enhanced immune evasion of SARS-CoV-2 variants KP.3.1.1 and XEC through N-terminal domain mutations. *Lancet Infect. Dis.* **25**, e6–e7 (2025).
54. Liu, J. et al. Virological and antigenic characteristics of SARS-CoV-2 variants LF.7.2.1, NP.1, and LP.8.1. *Lancet Infect. Dis.* **25**, e128–e130 (2025).
55. Li, H. et al. Establishment of replication-competent vesicular stomatitis virus-based recombinant viruses suitable for SARS-CoV-2 entry and neutralization assays. *Emerg. Microbes Infect.* **9**, 2269–2277 (2020).
56. Ye, J., Ma, N., Madden, T. L. & Ostell, J. M. IgBLAST: an immunoglobulin variable domain sequence analysis tool. *Nucleic Acids Res.* **41**, W34–W40 (2013).
57. Wickham, H. et al. Welcome to the Tidyverse. *J. Open Source Softw.* **4**, 1686 (2019).
58. Wickham, H. *Ggplot2: Elegant Graphics for Data Analysis* (Springer, 2016) https://doi.org/10.1007/978-3-319-24277-4
59. McInnes, L., Healy, J., Saul, N. & Großberger, L. UMAP: Uniform Manifold Approximation and Projection. *J. Open Source Softw.* **3**, 861 (2018).
60. Harris et al. Array programming with NumPy. *Nature* **585**, 357–362 (2020).
61. Hunter, J. D. Matplotlib: a 2D graphics environment. *Comput. Sci. Eng.* **9**, 90–95 (2007).
62. Virtanen, P. et al. SciPy 1.0: fundamental algorithms for scientific computing in Python. *Nat. Methods* **17**, 261–272 (2020).

Acknowledgements

We thank all volunteers who provided blood samples.

Author contributions

Y.C. designed and supervised the study. X.N. and Y.C. wrote the manuscript with input from all authors. X.N. and P.H. curated and analysed the epidemiological data. X.N., R.A. and Y.W. performed B cell sorting, 10x single-cell V(D)J sequencing experiments and data analysis. Q.W. performed plate-based single B cell V(D)J sequencing. X.N., Y.L., Xingan Cai, R.A., Y.W. and R.K. performed FACS analysis. J.W. and F.S. performed antibody expression. Y.Y. and P.H. constructed the pseudotyped virus and performed the pseudovirus infectivity assays. L.Y. performed the pseudovirus neutralization assays and ELISAs. F.J., P.H. and X.N. constructed the BA.3.2.2 mutant plasmids. D.X., Z.H., Tianyuan Zhao, X.T., Xiangpeng Chen, Z.X. and Juan Huang recruited the children cohort and collected the blood samples. B.Z., Tianen Zhu, Jianheng Huang and X.T. recruited the mRNA-vaccinated participants and collected the blood samples. Xiaosu Chen, Z.S. and R.J. recruited the randomly collected cohort and collected the blood samples.

Funding

This work was supported by the Chinese Academy of Sciences (to X.T.) and Changping Laboratory (2026D-04-01 to Y.C.). The funders had no role in study design, data collection and analysis, decision to publish or preparation of the manuscript.

Competing interests

Y.C. has international patent applications under the Patent Cooperation Treaty (PCT) for the BD series antibodies, including BD57-0553 and BD57-0968 (WO2024131774A9), and BD57-1169, BD57-1492 and BD57-1540 (WO2024131775A9). Y.C. is a co-founder of Singlomics Biopharmaceuticals. The other authors declare no competing interests.

Additional information

Extended data is available for this paper at https://doi.org/10.1038/s41564-026-02526-w.

Supplementary information The online version contains supplementary material available at https://doi.org/10.1038/s41564-026-02526-w.

Correspondence and requests for materials should be addressed to Xiangpeng Chen, Xiaotian Tan or Yunlong Cao.

Peer review information *Nature Microbiology* thanks the anonymous reviewer(s) for their contribution to the peer review of this work. Peer reviewer reports are available.

Reprints and permissions information is available at www.nature.com/reprints.

Publisher's note Springer Nature remains neutral with regard to jurisdictional claims in published maps and institutional affiliations.

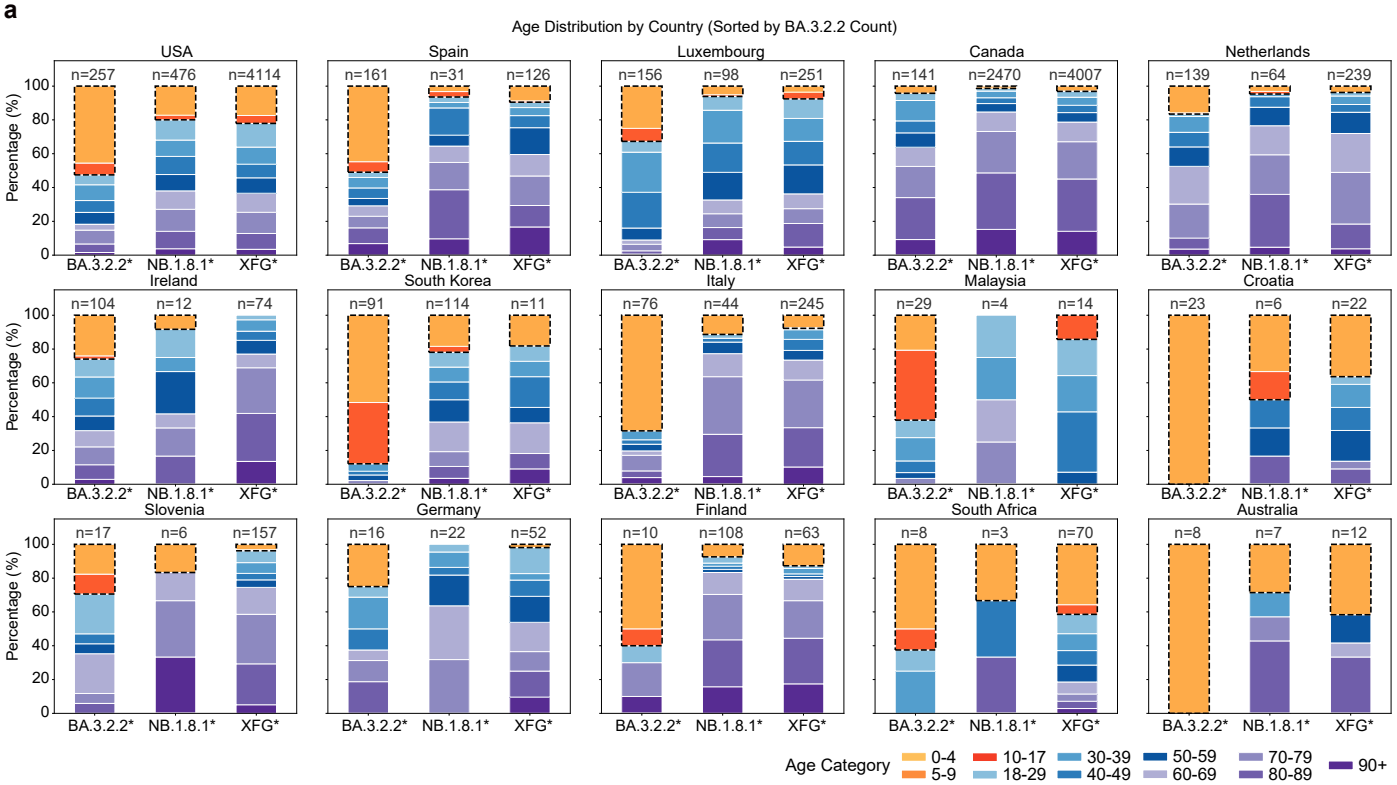
Open Access This article is licensed under a Creative Commons Attribution-NonCommercial-NoDerivatives 4.0 International License, which permits any non-commercial use, sharing, distribution and reproduction in any medium or format, as long as you give appropriate credit to the original author(s) and the source, provide a link to the Creative Commons licence, and indicate if you modified the licensed material. You do not have permission under this licence to share adapted material derived from this article or parts of it. The images or other third party material in this article are included in the article's Creative Commons licence, unless indicated otherwise in a credit line to the material. If material is not included in the article's Creative Commons licence and your intended use is not permitted by statutory regulation or exceeds the permitted use, you will need to obtain permission directly from the copyright holder. To view a copy of this licence, visit http://creativecommons.org/licenses/by-nc-nd/4.0/.

© The Author(s) 2026

[1]Biomedical Pioneering Innovation Center (BIOPIC), School of Life Sciences, Peking University, Beijing, People's Republic of China. [2]Changping Laboratory, Beijing, People's Republic of China. [3]College of Chemistry and Molecular Engineering, Peking University, Beijing, People's Republic of China. [4]Women and Children's Health Care Hospital of Luohu, Guangdong, People's Republic of China. [5]Beijing Key Laboratory of Core Technologies for the Prevention and Treatment of Emerging Infectious Diseases in Children, Key Laboratory of Major Diseases in Children, Ministry of Education, National Clinical Research Center for Respiratory Diseases, Laboratory of Infection and Virology, Beijing Pediatric Research Institute, Beijing Children's Hospital, Capital Medical University, National Center for Children's Health, Beijing, People's Republic of China. [6]Shenzhen Institutes of Advanced Technology, Chinese Academy of Sciences, Guangdong, People's Republic of China. [7]Shenzhen University General Hospital, Guangdong, People's Republic of China. [8]Shenzhen University, Guangdong, People's Republic of China. [9]Medical Laboratory of Shenzhen Luohu People's Hospital, Guangdong, People's Republic of China. [10]Institute for Immunology, College of Life Sciences, Nankai University, Tianjin, People's Republic of China. [11]Organ Transplant Center, NHC Key Laboratory for Critical Care Medicine, Tianjin First Central Hospital, Nankai University, Tianjin, People's Republic of China. [12]Beijing Ditan Hospital, Capital Medical University, Beijing, People's Republic of China. [13]Peking–Tsinghua Center for Life Sciences, Peking University, Beijing, People's Republic of China. [14]These authors contributed equally: Xiao Niu, Dan Xiong. ✉e-mail: chenxp1111@163.com; xt.tan@siat.ac.cn; yunlongcao@pku.edu.cn

https://doi.org/10.1038/s41564-026-02526-w

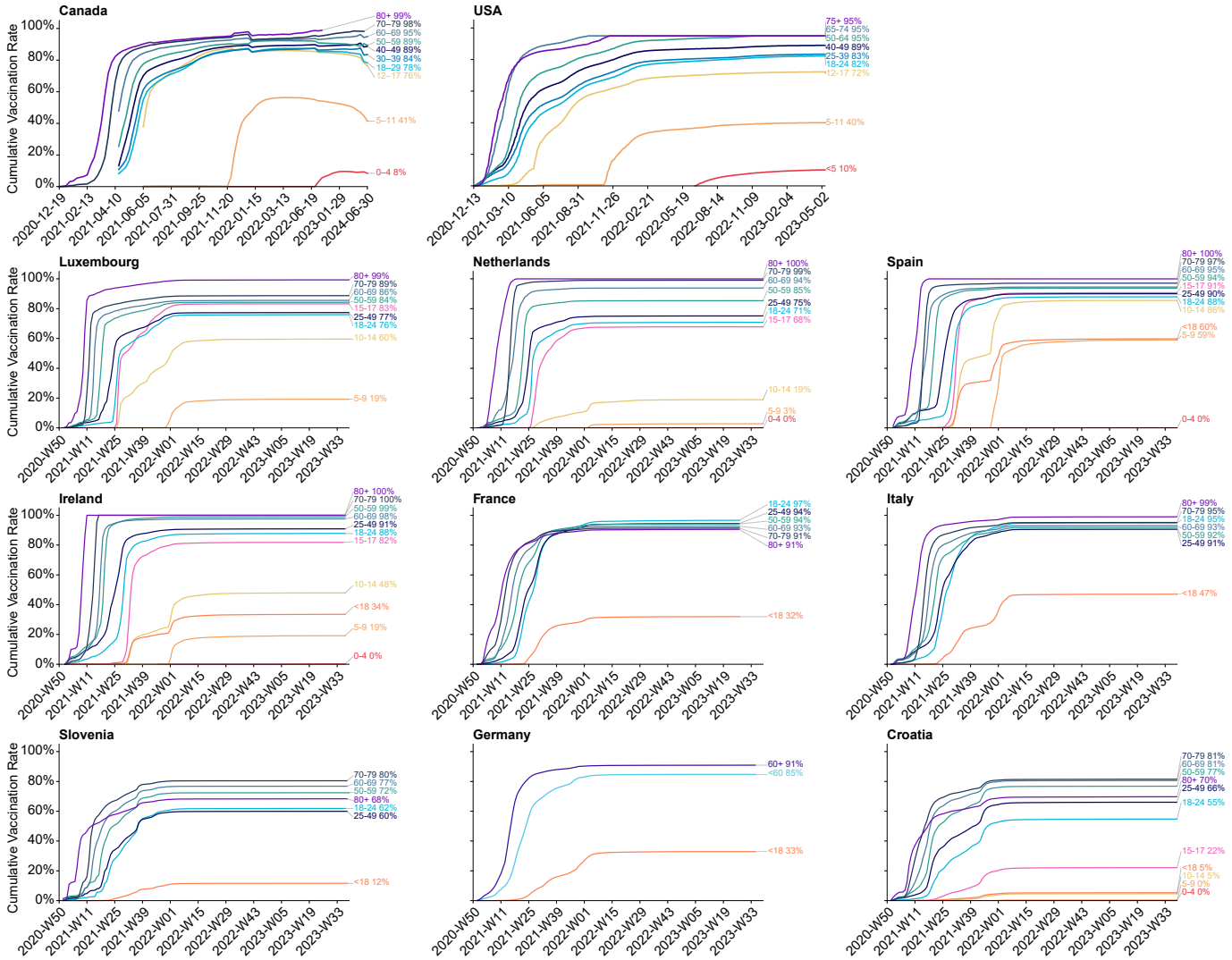
a



Extended Data Fig. 1 | Country-level surveillance confirms the paediatric enrichment of BA.3.2.2. a, Bar plots showing the age distribution of BA.3.2.2, NB.1.8.1 and XFG sublineages across countries. The group aged 17 years or younger is circled with black dashed outlines. Data were obtained from GISAID and include sequences collected between 1 December 2025 and 24 May 2026. Data processing is described in the Methods. An asterisk following a lineage name (BA.3.2.2*, NB.1.8.1* and XFG*) denotes the parental lineage together with all of its designated descendant lineages. n represents the number of individual records included in the corresponding GISAID analysis.

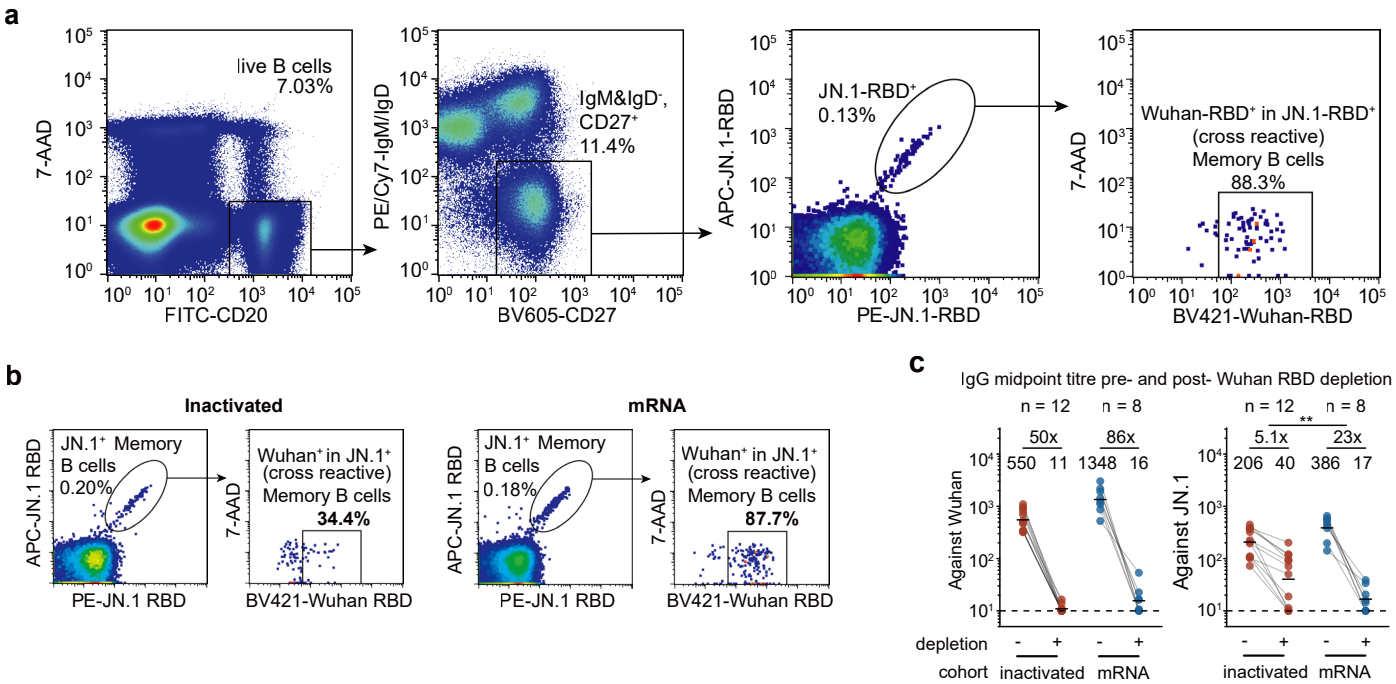
https://doi.org/10.1038/s41564-026-02526-w

a



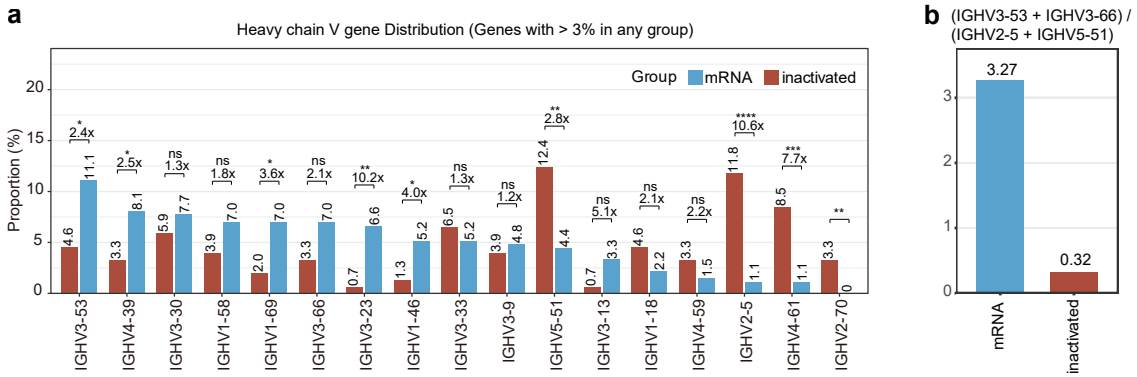
Extended Data Fig. 2 | Children show consistently lower vaccine coverage across countries. a, Temporal changes in vaccine coverage across age groups in major countries. Vaccination data were obtained from ECDC, the US CDC and canada.ca.

https://doi.org/10.1038/s41564-026-02526-w



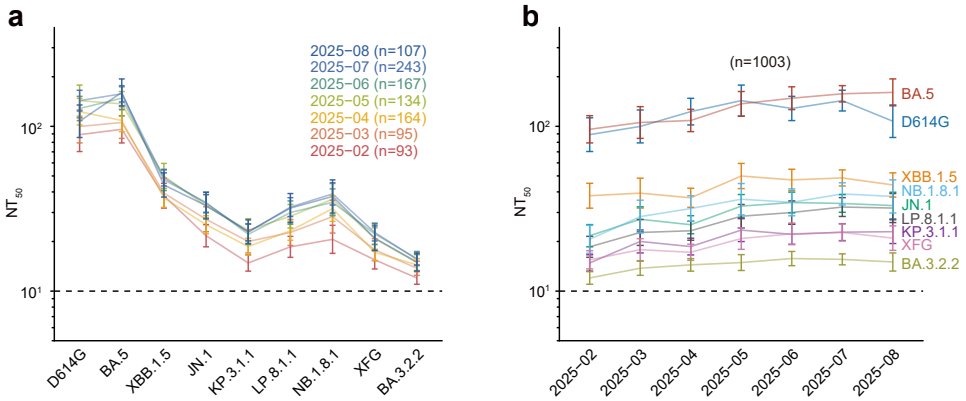
Extended Data Fig. 3 | Cellular and serological profiling validates stronger ancestral imprinting in mRNA-vaccinated individuals. a, Representative gating strategy for sorting human B cells. FITC, fluorescein isothiocyanate; BV605, Brilliant Violet 605; PE/Cy7, PE/Cyanine7. **b**, Representative flow cytometry dot plots of cross-reactive memory B cells from the inactivated-only (top) and mRNA-vaccinated (bottom) cohorts. APC, allophycocyanin; PE, phycoerythrin; BV421, Brilliant Violet 421. **c**, Plasma IgG midpoint titre against Wuhan (left) or JN.1 (right) RBD before and after Wuhan RBD depletion. Geometric mean values are displayed as bars and indicated above each group of data points. Statistical significance of the fold-reduction in titres was assessed between two cohorts. Dashed lines indicate the limit of detection (midpoint titre = 10). In **c**, n represents the number of individual participants. The ELISA assays were conducted in at least two independent experiments. Two-sided Wilcoxon rank-sum tests were used in **c**. *P < 0.05, **P < 0.01, ***P < 0.001, ****P < 0.0001; ns, not significant (P > 0.05).

https://doi.org/10.1038/s41564-026-02526-w



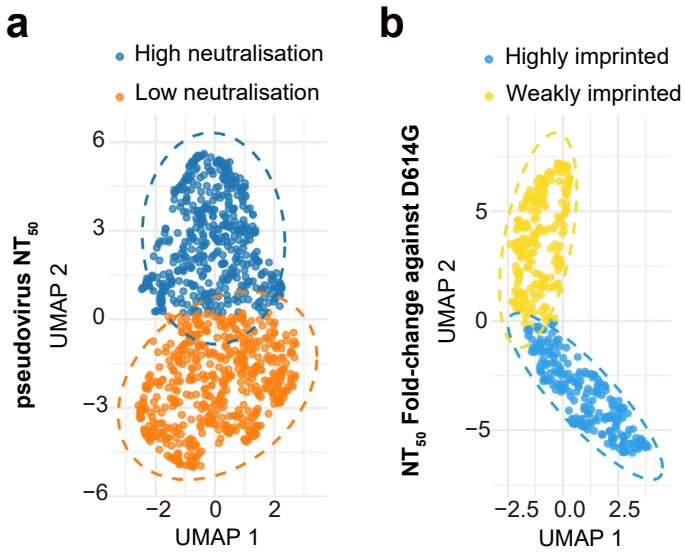
Extended Data Fig. 4 | IGHV gene usage distinguishes highly and weakly imprinted antibody repertoires. a, Frequency of heavy chain V gene usage among JN.1 RBD-reactive memory B cells of the two cohorts. **b**, Bars show the ratio of the combined usage of *IGHV3-53* and *IGHV3-66* to the combined usage of *IGHV2-5* and *IGHV5-51* within each group. Two-sided Fisher's exact tests were used when any expected cell count was <5; otherwise, two-sided chi-square tests were used in **a**. *P < 0.05, **P < 0.01, ***P < 0.001, ****P < 0.0001; ns, not significant (P > 0.05).

https://doi.org/10.1038/s41564-026-02526-w



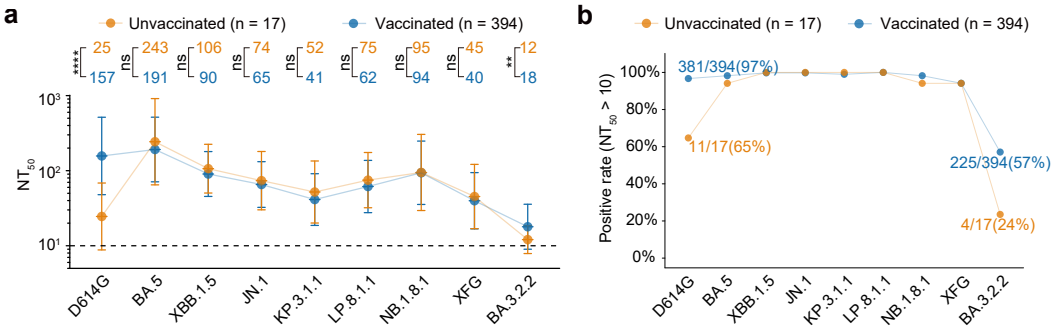
Extended Data Fig. 5 | Temporal increases in plasma neutralisation responses across the sampled population. a-b, Temporal changes in sampling time and plasma neutralising antibody responses against a panel of SARS-CoV-2 variant pseudoviruses. Geometric mean titres (GMTs) are shown on the top. Dashed lines indicate the limit of detection (NT50 = 10). Data are presented as geometric mean titres (GMT), with error bars indicating geometric standard deviation. In **a**–**b**, n represents the number of individual participants. Neutralisation assays were conducted in at least two independent experiments. a and b can be reproduced using the data provided in Supplementary Table 2 as the source data.

https://doi.org/10.1038/s41564-026-02526-w



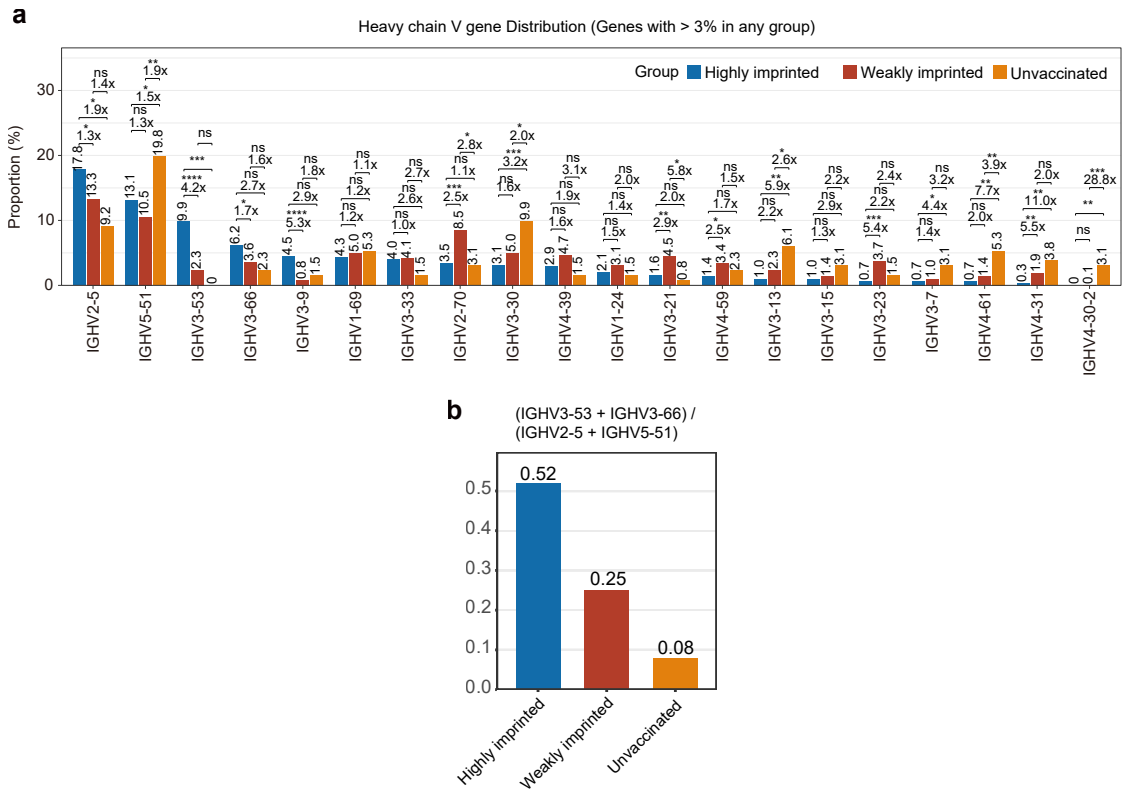
Extended Data Fig. 6 | Neutralisation-based UMAP clustering identifies imprinting-associated population groups. a-b, Uniform manifold approximation and projection (UMAP) projection showing clusters based on pseudovirus NT50 (**a**) and NT50 fold changes against D614G (**b**). **a** and **b** can be reproduced using the data provided in Supplementary Table 2 as the source data.

https://doi.org/10.1038/s41564-026-02526-w



Extended Data Fig. 7 | Unvaccinated individuals retain Omicron neutralisation but show reduced BA.3.2.2 activity. a, NAb response of the unvaccinated and vaccinated individuals against a panel of SARS-CoV-2 variant pseudoviruses. Geometric mean titres (GMTs) are shown on the top. Dashed lines indicate the limit of detection (NT50 = 10). Data are presented as geometric mean titres (GMT), with error bars indicating geometric standard deviation. **b**, Plasma neutralisation positivity rates for the data shown in a. Positivity was defined as a titre above the limit of detection (NT50 = 10). In **a**–**b**, n represents the number of individual participants. Only participants with a clearly documented vaccination history were included in this analysis. Neutralisation assays were conducted in at least two independent experiments. Two-sided Wilcoxon rank-sum tests were used in a. *P < 0.05, **P < 0.01, ***P < 0.001, ****P < 0.0001; ns, not significant (P > 0.05).

https://doi.org/10.1038/s41564-026-02526-w



Extended Data Fig. 8 | Expanded population BCR profiling supports imprinting-dependent IGHV usage. a, Frequency of heavy-chain V gene usage in the highly imprinted, weakly imprinted and unvaccinated cohorts. **b**, Bars show the ratio of the combined usage of *IGHV3-53* and *IGHV3-66* to the combined usage of *IGHV2-5* and *IGHV5-51* within each group. Two-sided Fisher's exact tests were used when any expected cell count was <5; otherwise, two-sided chi-square tests were used in a. *P < 0.05, **P < 0.01, ***P < 0.001, ****P < 0.0001; ns, not significant (P > 0.05).

nature portfolio

Corresponding author(s): Yunlong Cao

Last updated by author(s): Sep 13, 2026

Reporting Summary

Nature Portfolio wishes to improve the reproducibility of the work that we publish. This form provides structure for consistency and transparency in reporting. For further information on Nature Portfolio policies, see our Editorial Policies and the Editorial Policy Checklist.

Statistics

For all statistical analyses, confirm that the following items are present in the figure legend, table legend, main text, or Methods section.

n/a	Confirmed	
☐	☒	The exact sample size (*n*) for each experimental group/condition, given as a discrete number and unit of measurement
☐	☒	A statement on whether measurements were taken from distinct samples or whether the same sample was measured repeatedly
☐	☒	The statistical test(s) used AND whether they are one- or two-sided *Only common tests should be described solely by name; describe more complex techniques in the Methods section.*
☒	☐	A description of all covariates tested
☐	☒	A description of any assumptions or corrections, such as tests of normality and adjustment for multiple comparisons
☐	☒	A full description of the statistical parameters including central tendency (e.g. means) or other basic estimates (e.g. regression coefficient) AND variation (e.g. standard deviation) or associated estimates of uncertainty (e.g. confidence intervals)
☐	☒	For null hypothesis testing, the test statistic (e.g. *F*, *t*, *r*) with confidence intervals, effect sizes, degrees of freedom and *P* value noted *Give P values as exact values whenever suitable.*
☒	☐	For Bayesian analysis, information on the choice of priors and Markov chain Monte Carlo settings
☒	☐	For hierarchical and complex designs, identification of the appropriate level for tests and full reporting of outcomes
☒	☐	Estimates of effect sizes (e.g. Cohen's *d*, Pearson's *r*), indicating how they were calculated

Our web collection on statistics for biologists contains articles on many of the points above.

Software and code

Policy information about availability of computer code

Data collection	Pseudovirus neutralization data were acquired using a microplate spectrophotometer (PerkinElmer, HH3400). ELISA data were collected using a Multiskan FC microplate reader (Thermo Scientific). Flow cytometry data were acquired on a Symphony A5SE cytometer (BD Biosciences) and a MoFlo Astrios EQ Cell Sorter (Beckman Coulter).
Data analysis	Data analysis and visualization were performed using standard software or packages/libraries in R v4.3.2 or Python v3.10.11, including tidyverse v2.0.0, ggplot2 v3.5.1, and umap v0.2.10.0 in R, and NumPy v1.26.4, Matplotlib v3.8.4, and SciPy v1.13.0 in Python. SARS-CoV-2 lineage annotations were curated using metadata from GISAID and lineage_notes.txt and alias_key.json from the cov-lineages/pango-designation GitHub repository. No custom algorithms or software were developed.

For manuscripts utilizing custom algorithms or software that are central to the research but not yet described in published literature, software must be made available to editors and reviewers. We strongly encourage code deposition in a community repository (e.g. GitHub). See the Nature Portfolio guidelines for submitting code & software for further information.

Data

Policy information about availability of data

All manuscripts must include a data availability statement. This statement should provide the following information, where applicable:

- Accession codes, unique identifiers, or web links for publicly available datasets
- A description of any restrictions on data availability
- For clinical datasets or third party data, please ensure that the statement adheres to our policy

Information on individuals providing blood samples and neutralisation titres involved in this study has been included in Supplementary Tables 1 and 2. The paired B-cell receptor sequences generated by plate-based single B-cell sequencing from human samples and the primers used are provided in Supplementary Table 3. The processed productive amino acid sequences obtained from the 10x Genomics single-cell V(D)J sequencing data are provided in Supplementary Table 4. The raw 10x Genomics single-cell V(D)J sequencing reads generated in this study have been deposited in the CNGB Sequence Archive (CNSA) under accession number CNP0009821 and in the Genome Sequence Archive for Human (GSA-Human) at the National Genomics Data Center, China National Center for Bioinformation, under accession number HRA020962 (BioProject: PRJCA073984). Requests for resources and reagents should be directed to and will be fulfilled by the lead contact, yunlongcao@pku.edu.cn (Y.C.) and are subject to a Material and Data Transfer Agreement. All enquiries will be replied to within one week. Source data are provided with this paper.

Research involving human participants, their data, or biological material

Policy information about studies with human participants or human data. See also policy information about sex, gender (identity/presentation), and sexual orientation and race, ethnicity and racism.

Reporting on sex and gender	The study included 1055 human participants, including 429 males and 626 females. Participants were assigned to 4 groups: mRNA-vaccinated (n = 8), inactivated-only (n = 12), Random cohort (n = 1003) and children cohort (n = 32). Participant age, sex and SARS-CoV-2 vaccination/infection history are provided in Supplementary Tables 1 and 2. The study was not designed or powered to assess sex- or gender-specific differences in immune responses, and no sex- or gender-based analyses were performed. Findings are therefore not intended to be interpreted as sex- or gender-specific. Information of the human participants involved in this study is included in Supplementary Table.
Reporting on race, ethnicity, or other socially relevant groupings	Information on race, ethnicity, or other socially relevant groupings was not collected for human participants in this study. As such, no analyses stratified by race or ethnicity were performed.
Population characteristics	Participants included convalescent adult individuals, a random cohort, and a children cohort. The inactivated-only cohort (n = 12) received three doses of CoronaVac, with samples collected 46.5 ± 5.4 months after the first vaccine dose. The mRNA-vaccinated cohort (n = 8) received at least one mRNA vaccine dose (BNT162b2 or mRNA-1273), with samples collected 46.0 ± 2.3 months after initial vaccination. The random cohort included 1,003 participants. The children cohort included 32 participants. Detailed infection histories were unavailable for some participants.
Recruitment	A total of 1,055 participants were recruited through clinical networks and classified into four groups: mRNA-vaccinated (n = 8), inactivated-only (n = 12), a random cohort (n = 1,003), and a children cohort (n = 32). The 1,003 samples in the random cohort were collected specifically for this study and were not obtained as part of routine clinical care. For this cohort, eligibility was restricted to individuals without immunodeficiency or related conditions. Recruitment and sampling were conducted in Beijing and Tianjin and may therefore be subject to geographic sampling bias. The targeted paediatric and adult cohorts showed expected age imbalances related to their prespecified recruitment and vaccination-history criteria, and the broader randomly sampled cohort showed a moderate female predominance. We are not aware of any additional recruitment bias. The inclusion criteria were: (1) documented histories of SARS-CoV-2 infection and vaccination and (2) willingness of participants and their legal guardians, where applicable, to participate and provide signed written informed consent. Individuals were excluded if they met any of the following criteria: (1) HIV infection, active hepatitis, or active tuberculosis; (2) a history of bone marrow transplantation or ongoing cancer radiotherapy or chemotherapy; (3) current use of immunosuppressive agents; (4) immunodeficiency caused by definitive genetic defects; (5) receipt of stem-cell therapy within the preceding six months; (6) current receipt of antibody therapy; (7) acute or chronic infection; (8) malignancy or other tumors; or (9) any other condition deemed unsuitable for the study by the investigators. Written informed consent was obtained from all adult participants before sample collection, and written informed consent was obtained from the parents or legal guardians of minor participants. All participants who completed collection of blood sample received compensation.
Ethics oversight	The paediatric cohort was approved by the Institutional Review Board of Shenzhen Luohu People's Hospital (ethics approval no. 2260206006) and the Ethics Committee of Beijing Children's Hospital, Capital Medical University (IEC-C-006-A04-V.08). The population sampling cohort was approved by the Ethics Committee of Tianjin First Central Hospital (KEYAN20241022-2) and the Institutional Review Board of Beijing Ditan Hospital, Capital Medical University (DTEC-KY2024-112-01). The mRNA-vaccinated cohort was approved by the Institutional Review Board of Shenzhen Institutes of Advanced Technology, Chinese Academy of Sciences (SIAT-IRB-230715-H0667), and the inactivated-vaccine cohort was approved by the Institutional Review Board of Beijing Ditan Hospital, Capital Medical University (DTEC-KY2024-112-01). All participants provided their agreement for the collection, storage and use of their blood samples strictly for research purposes and the subsequent publication of related data. Written informed consent was obtained from all adult participants. For participants who were minors, written informed consent was obtained from their parents or legal guardians. All participants received compensation for participation.

Note that full information on the approval of the study protocol must also be provided in the manuscript.

Field-specific reporting

Please select the one below that is the best fit for your research. If you are not sure, read the appropriate sections before making your selection.

☒ Life sciences ☐ Behavioural & social sciences ☐ Ecological, evolutionary & environmental sciences

For a reference copy of the document with all sections, see nature.com/documents/nr-reporting-summary-flat.pdf

Life sciences study design

All studies must disclose on these points even when the disclosure is negative.

Sample size	The study involved 87 SARS-CoV-2 RBD-targeting Class 1 and Class 1/4 monoclonal antibodies and included 1,055 human participants. The sample sizes were determined by the number of available mAbs and eligible participants and were not predetermined. No statistical methods were used to predetermine sample sizes, but our sample sizes are similar to those reported in previous publications
Data exclusions	For the epidemiological analyses, GISAID records with missing or non-informative collection date, location, patient age, or lineage information were excluded. Records with unparseable or clearly erroneous ages, as well as broad age intervals crossing the prespecified age-group boundaries, were also excluded from age-distribution analyses. France was excluded from the age-distribution analyses because a large proportion of records reported age only as broad intervals crossing these boundaries. For the harmonised vaccination-coverage analyses, age strata that overlapped, crossed prespecified category boundaries, or could not be unambiguously assigned to a single harmonised age group were excluded to avoid double counting or arbitrary allocation.
Replication	Experimental assays were performed in at least two independent experiments. Replication attempts were successful and results were consistent across replicates.
Randomization	As this was an observational study, participants were not randomized to experimental groups, and no additional randomization or blocking was applied during sample processing or experimental assays.
Blinding	Investigators performing the experimental assays were not blinded to participant group information during data collection; statistical analyses were not performed blind to group allocation.

Reporting for specific materials, systems and methods

We require information from authors about some types of materials, experimental systems and methods used in many studies. Here, indicate whether each material, system or method listed is relevant to your study. If you are not sure if a list item applies to your research, read the appropriate section before selecting a response.

Materials & experimental systems

n/a	Involved in the study
☐	☒ Antibodies
☐	☒ Eukaryotic cell lines
☒	☐ Palaeontology and archaeology
☒	☐ Animals and other organisms
☒	☐ Clinical data
☒	☐ Dual use research of concern
☒	☐ Plants

Methods

n/a	Involved in the study
☒	☐ ChIP-seq
☐	☒ Flow cytometry
☒	☐ MRI-based neuroimaging

Antibodies

Antibodies used	Goat anti-Mouse IgG (H+L) Cross-Adsorbed Secondary Antibody (Invitrogen, G21040) Peroxidase AffiniPure Goat Anti-Human IgG (H+L) (Jackson ImmunoResearch, 109-035-003) FITC anti-human CD20 (BioLegend, 302304) Brilliant Violet 605™ anti-human CD27 (BioLegend, 302824) PE/Cyanine7 anti-human IgM (BioLegend, 314532) PE/Cyanine7 anti-human IgD (BioLegend, 348210) Custom human monoclonal antibodies were expressed in-house using Expi293F cells (Thermo Fisher, A14527) with codon-optimized cDNA and human IgG1 constant regions. For ELISA, 100 µL of the appropriate HRP-conjugated secondary antibody was used per well and incubated for 30 minutes at room temperature. Custom human monoclonal antibodies were serially diluted from an initial concentration of 1 µg/mL, and 100 µL of each dilution was used. For flow cytometric staining, 3 µL per 100 µL of FITC anti-human CD20 and Brilliant Violet 605™ anti-human CD27 antibodies, and 2 µL per 100 µL of PE/Cyanine7 anti-human IgM and PE/Cyanine7 anti-human IgD antibodies were used. For the neutralization assay, custom human monoclonal antibodies were serially diluted from an initial dilution of 1:50–1:100.

Validation	Commercially available antibodies were validated by the manufacturers as follows: https://www.thermofisher.cn/cn/zh/antibody/product/Goat-anti-Mouse-IgG-H-L-Cross-Adsorbed-Secondary-Antibody-Polyclonal/G-21040 https://www.jacksonimmuno.com/catalog/products/109-035-003 https://www.biolegend.com/en-gb/products/fitc-anti-human-cd20-antibody-558 https://www.biolegend.com/en-gb/products/brilliant-violet-605-anti-human-cd27-antibody-7804?GroupID=BLG10174 https://www.biolegend.com/en-gb/products/pe-cyanine7-anti-human-igm-antibody-12467 https://www.biolegend.com/en-gb/products/pe-cyanine7-anti-human-igd-antibody-6996

Eukaryotic cell lines

Policy information about cell lines and Sex and Gender in Research

Cell line source(s)	Monoclonal antibody expression: Expi293F™ (ThermoFisher, A14527); Pseudutyped virus neutralization assay: Huh-7 (JCRB, 0403) ; Pseudutyped virus production: 293T(ATCC, CRL-3216); Pseudotyped virus infectivity assay: Vero E6 (ATCC, CRL-1586/VERO C1008)
Authentication	Expi293F™ (ThermoFisher, A14527): https://assets.thermofisher.cn/TFS-Assets/certificate/CM/COA/COA_A14527_3083222_1.pdf; Huh-7 (JCRB 0403): https://cellbank.nibiohn.go.jp/~cellbank/en/search_res_det.cgi?ID=385); 293T(ATCC, CRL-3216): STR profiling (https://www.atcc.org/products/crl-3216); Vero E6 (ATCC, CRL-1586/VERO C1008): https://www.atcc.org/products/crl-1586
Mycoplasma contamination	Not tested for mycoplasma contamination;
Commonly misidentified lines (See ICLAC register)	No commonly misidentified cell lines were used in the study.

Plants

Seed stocks	N/A
Novel plant genotypes	N/A
Authentication	N/A

Flow Cytometry

Plots

Confirm that:

☒ The axis labels state the marker and fluorochrome used (e.g. CD4-FITC).

☒ The axis scales are clearly visible. Include numbers along axes only for bottom left plot of group (a 'group' is an analysis of identical markers).

☒ All plots are contour plots with outliers or pseudocolor plots.

☒ A numerical value for number of cells or percentage (with statistics) is provided.

Methodology

Sample preparation	PBMCs and plasma were isolated from human blood samples using Ficoll (Cytiva, 17-1440-03) density gradient centrifugation. B cells were enriched from PBMCs using a CD19+ positive selection kit (STEMCELL, 17854). The enriched B cells were then stained with JN.1 RBD (Sino Biological, 40592-V49H16-B) and Wuhan RBD (Sino Biological, 40592-V27H-B). B cells were also stained with antibodies against CD20 (BioLegend, 302304), CD27 (BioLegend, 302824), IgM (BioLegend, 314532), IgD (BioLegend, 348210) and 7-AAD (Invitrogen, 00-6993-50).
Instrument	Flow cytometry data were acquired on MoFlo Astrios EQ Cell Sorter (Beckman Coulter).
Software	Flow cytometry data were acquired using MoFlo Astrios EQ Cell Sorter (Beckman Coulter, Summit 6.0 software). Data analysis was performed using FlowJo v10.8 (BD Biosciences).
Cell population abundance	The relative abundance of the sorted population within the starting material was determined based on flow cytometric frequencies, as defined by the antigen-binding gate. For human samples, antigen-positive memory B cells were defined as

7AAD- CD20+ CD27+ IgD- IgM- RBD+ cells. These cells constituted approximately 0.0005% of total live singlet cells prior to sorting.

Gating strategy

A consistent sequential gating strategy was applied to all samples. Cells were first gated based on forward scatter (FSC-A) versus side scatter (SSC-A) to exclude debris, followed by FSC-H versus FSC-W gating to remove doublets and select single cells. Dead cells were excluded using 7-AAD.
For human samples, live singlet cells were gated on CD20 to define B cells, followed by selection of CD27+ IgD- IgM- memory B cells. Antigen-specific cells were identified by RBD binding (Wuhan or JN.1).
Boundaries between positive and negative populations were initially determined using fluorescence-minus-one (FMO) controls, unstained controls, and non-immunized controls. To account for potential signal shifts related to instrument performance, gates were fine-tuned for individual samples based on clear population clusters/separations where evident, while maintaining the overall gating hierarchy established prior to analysis.

☒ Tick this box to confirm that a figure exemplifying the gating strategy is provided in the Supplementary Information.